*GEOCHEMISTRY INTERNATIONAL, 2025, Vol. 70, No. 1, pp. 38–60*

# THE ARCHEAN AGE OF GRANITE-GNEISS COMPLEXES FROM THE KAMA-VYATKA ZONE (THE VOLGA-URAL SEGMENT, EAST EUROPEAN CRATON)

**©2025 M. O. Anosova[a,*], O. V. Astrakhantsev[a], A. V. Postnikov[b], A. A. Fedotova[a], T. I. Kirnozova[a], M. M. Fugzan[a], and I. A. Sabirov[b]**

[a] *Vernadsky Institute of Geochemistry and Analytical Chemistry, Russian Academy of Sciences, Moscow, Russia*
[b] *Gubkin Russian State University of Oil and Gas, Moscow, Russia*
**e-mail: anosova@geokhi.ru*

Received February 03, 2024
Revised July 07, 2024
Accepted August 23, 2024

**Abstract.** The formation history of granulite complexes is fundamental to understanding the processes of early continental crust origins. The work presents the results of an isotope-geochronological study of rock samples from the main complexes of the Kama-Vyatka zone (the Volga-Ural segment, the East European craton) — enderbites of the Otradnensky series and quartz diorites of the Tanai plagiogranitoid massif. The Sm–Nd isotopic data were used to calculate model ages of quartz diorites of the Tanaysky plagiogranitoid massif and enderbites of the Otdnenskaya series — 3.2 and 3.0 Ga, respectively. The U–Pb isotope system of zircon was investigated by LA-ICP-MS. The zircon of quartz diorites indicated the Archean age of protolith formation of the plagiogranitoids of the Tanaysky Massif. This time interval — 3.04–2.98 Ga — includes the stage of the earliest granulite metamorphism immediately following the episode of magmatism. There are several generations of zircon grains from a sample of weakly gneissed enderbites of the Otradnensky series in the 3.0–2.8 Ga age interval, which record the following events: the formation of primary enderbites, locally manifested partial melting under granulite facies conditions and regressive stage of metamorphism in the transitional conditions of granulite to amphibolite facies. Considering to model age of enderbites, for the first time, an estimate of the age of the Otradnensky Group of the Kama-Vyatka zone of the Volga-Ural segment was obtained — 3.0 ± 0.1 Ga. In the 2.75–2.60 Ga age interval, zircon from a sample of weakly gneissed enderbites records the most significant episode of granulite metamorphism, widely manifested throughout the Volga-Ural segment and, replacing it, regressive metamorphism with the input of water-bearing fluid and temperature decreasing

**Keywords:** *Archean, Proterozoic, zircon, U–Pb isotope system, geochronology, Volga-Ural segment, enderbites, granulites, Sm-Nd, model age*

**DOI:** 10.31857/S00167525250102e2

## INTRODUCTION

Determining the sequence of magmatic and metamorphic processes and the timing of their manifestation allows understanding the mechanisms of ancient continental crust formation, which remain subjects of debate (for example, Belousova et al., 2010; Condie, 2018; Hawkesworth et al., 2010, 2020). The timing of maximum areal granulite metamorphism is a key parameter for reconstructions, as researchers correlate it with the time of continental crust stabilization (Hawkesworth et al., 2010). Methods of local U–Pb isotope analysis provide the opportunity to study different-aged zones of zircon. At the same time, approaches to interpreting isotope-geochemical data obtained from zircon, and their correlation with crystallization and recrystallization processes of rocks, including those that have repeatedly undergone metamorphism, are not always obvious (Whitehouse, Kamber, 2005; Kaulina, 2010; Glebovitsky et al., 2008; Kohn, Kelly, 2018; Kunz et al., 2018). The absence of direct data on the age of rocks from

the Kama-Vyatka zone, one of the most extended structures of the crystalline basement of the Volga-Ural segment of the East European Craton (hereinafter EEC) (Bogdanova, 1986; Bogdanova, Gorbatschev, 2016), has hindered the deciphering of the region's geological development history.

The task of this study was to determine the age of rocks of the two most common structural-material complexes of the Kama-Vyatka zone – weakly gneissic enderbites of the Otradnensky series, representing the granulite complex (sample Pr 143-1) and metamorphosed quartz diorites of the Tanai plagiogranitoid massif (sample TB 238-4) (Fig. 1). Sm–Nd isotopic characteristics were studied and model ages were calculated, providing an opportunity to characterize the protolith of these rocks. The work is based on the interconnected study of petrographic features of polychronic metamorphic rocks, morphology and internal structure of zircon crystals, Th and U contents, and data from isotopic U–Pb zircon analysis. The results allowed determining the time of formation and recrystallization of rocks of the main structural-material complexes of the Kama-Vyatka zone, and examining the problem of reconstructing the early stages of continental crust formation in the Volga-Ural segment of the EEC.

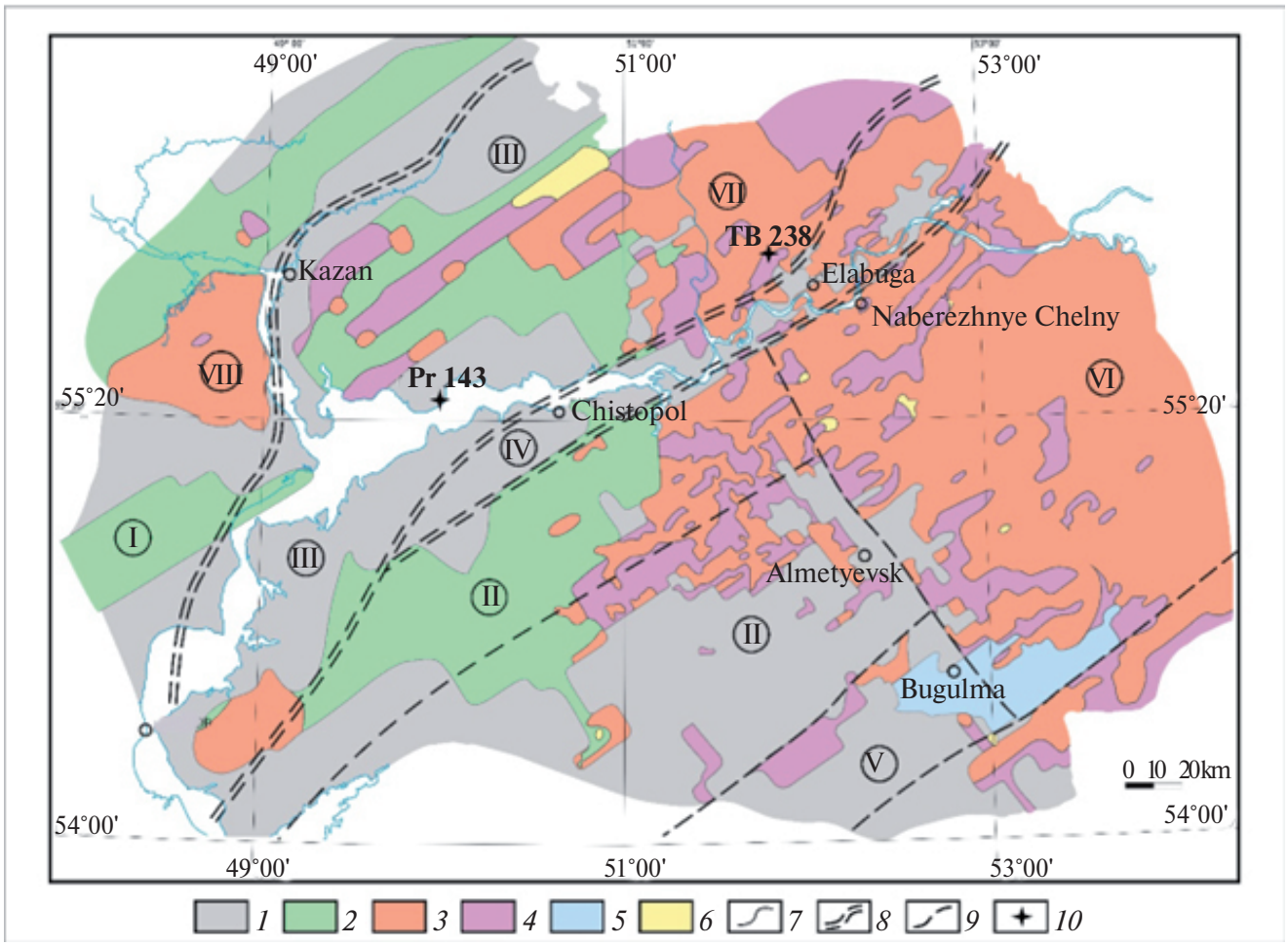


**Fig. 1.** Scheme of the geological structure of the crystalline basement of Tatarstan (*based on materials by A.V. Postnikov and S.V. Bogdanova*) (Bogdanova, 1986; Bibikova et al., 2015; Bogdanova et al., 2016, Pre-platform..., 1992):
Legend: *1* – granulite-gneisses of the Otradnensky series, *2* – biotite-amphibole plagiogneisses undifferentiated, *3* – granitoid and granite-gneiss complexes, *4* – migmatite zones, *5* – anorthosites of the Tuimazin massif, *6* – volcanic-sedimentary strata of the Archean and Early Proterozoic, *7* – geological boundaries, *8–9* – boundaries of large tectonic blocks and linear fold zones: *8* – first order, *9* – second order, *10* – locations of wells.
Roman numerals – tectonic elements of the crystalline basement of Tatarstan. Tectonic blocks: I – Tokmov block, II – South Tatar block of the Middle Volga megablock; Linear-fold zones: III – Kama-Vyatka zone, IV – Yelabuga zone, V – Zhigulevsk-Tuimazin belt; Granitoid and gneiss-granite complexes: VI – Bakalinsky gneiss-granite massif, VII – Tanai plagiogranitoid massif, VIII – Sviyazhsk granitoid massif.

## GEOLOGICAL STRUCTURE

The Volga-Ural segment is one of the three main components of the East European craton (Bogdanova, 1993; Bogdanova et al., 2016). The Volga-Ural segment represents an area of areal distribution of predominantly Archean rocks that experienced tectonothermal reworking under conditions of granulite and amphibolite facies metamorphism during the Meso-, Neoarchean and Paleoproterozoic times.

Archean rocks are represented by granulite-gneisses of the Otradnensky series, high-alumina gneisses and crystalline schists of the Bolshecheremshansk series (Fig. 1). The latter are considered supracrustal formations. The eastern part of the Volga-Ural segment of the East European craton is composed of granite-gneiss complexes of the Bakalinsky and Tanai massifs (Bogdanova, 1986; Bibikova et al., 2015; Doplatformennye..., 1992 ).

Due to the widespread development of a thick (1.5–3 km) sedimentary cover within the Volga-Ural segment, data on the structure of the basement within it are based on drilling results and geophysical studies. Archean and Paleoproterozoic rocks form dome-block structures – megablocks, separated by Paleoproterozoic linear zones (Bogdanova, 1986; Pre-platform..., 1992). The largest of them are the Volga-Kama and Middle Volga megablocks (Bogdanova et al., 2016), which form the northwestern and southeastern parts of the Volga-Ural segment, respectively. They are separated by the Kama-Vyatka linear zone and the Vladimir-Kazan linear zone, which replaces it along the strike from northeast to southwest and west (Bogdanova, 1986; Pre-platform..., 1992; Bogdanova et al., 2016).

Crystalline complexes of the basement of the Kama-Vyatka zone are represented by two-pyroxene-plagioclase crystalline schists and gneisses, hypersthene-plagioclase gneisses, enderbite-gneisses of the Otradnensky series. In isolated cases, wells penetrate small bodies of gabbroids and small massifs of charnockitoids. The northeastern part of the studied territory is occupied by the Tanai massif, in which rocks of the granodiorite-plagiogranite series predominate. The latest intrusions are bodies of microcline granites that seal the Archaean and Paleoproterozoic structure of the Kama-Vyatka zone.

In terms of composition, the Kama-Vyatka zone gravitates towards the Middle Volga megablock, composed of rocks predominantly of Archaean age. Rock complexes typical for the Middle Volga megablock are recognized in the Kama-Vyatka zone along with rocks not identified or less common in the Middle Volga megablock (Bibikova et al., 2015).

The granulite-gneiss region of the Middle Volga megablock was formed, apparently, mainly in the Neoarchaean time. Magmatic formations of various compositions (enderbites, charnockitoids, quartz diorites) crystallized about 2.7 billion years ago (ID-TIMS data, (Bibikova et al., 1994)). However, a detailed study of magmatic and metasedimentary complexes allows identifying earlier episodes of crust formation. The Bakalinsky massif of the Middle Volga megablock, studied by U–Pb (ID–TIMS), U–Th–Pb (SIMS) and Lu–Hf methods, includes four complexes of granitoids, different in age, the rocks crystallized in the interval of 3.3–2.6 billion years (Bibikova et al., 2008; Bogdanova et al., 2010). The study of sections with dominant high-alumina gneisses, united in the Bolshaya Cheremshanka series (Lapinskaya, Bogdanova, 1976), by isotope-geochemical and geochronological methods (U–Pb data on detrital zircons and Sm–Nd data on rocks), showed that Early Archaean material is widely represented in the composition of the terrigenous protolith of metamorphic rocks of the Bolshaya Cheremshanka series. Detrital zircons with an age of more than 3 billion years have been identified (Bibikova et al., 2015).

Along the southeastern border of the Kama-Vyatka zone with the Middle Volga megablock, the Yelabuga belt of shear and thrust dislocations is distinguished. It represents a system of narrow tectonic wedges oriented according to the strike of the structures of the Kama-Vyatka linear zone. Faults and associated diaphthoresis zones cut through the Archean fold structure. There are clear signs of Paleoproterozoic restructuring of the Archean structural plan (Bogdanova, 1986; Fedotova et al., 2019).

## MATERIALS AND METHODS

### *Characteristics and petrographic description of samples*

The Tanai plagiogranitoid massif was studied using rocks exposed by the Tanai-Bekhterev well 238 in the interval 1772.7–1776.7 m (4 m), representing a typical basement section of the Kama-Vyatka zone of the Volga-Ural segment. The section is dominated by quartz diorites, transitioning in bands to biotite-hornblende (sometimes cummingtonite) plagiogneisses, and including thin (up to 2 cm) veins of plagiogranites (Fig. 2a, b, c, d). In some areas, primarily in leucocratic segregations, up to 15 vol. % of microcline is present.

For analysis, a sample of slightly gneissic and migmatized quartz diorite (hereinafter TB 238-4) was selected, having a medium-grained hypidiomorphic

granular texture, characterized by hypidiomorphic tabular grains of plagioclase (An 26–32) (45–50 vol. %), prismatic hornblende (15–20 vol. %) and lamellar biotite (10–15 vol. %) and xenomorphic quartz (15–20 vol. %). Accessory and ore minerals include zircon, apatite, allanite (orthite), magnetite.

The orientation of hornblende grains (pleochroism from light yellow to bottle green) and, especially, biotite (pleochroism from light yellow to dark brown, with a reddish tint) is partly subordinate to the direction of gneissosity.

The variable composition of plagioclase and the presence of weakly expressed zonation, in which antiperthitic inclusions are noted in the central parts of the grains, suggests the formation of the rock through reworking (partial melting?) of an enderbitic substrate (Fig. 2e).

Zircon grains can occur both between rock-forming mineral grains and as inclusions in biotite, surrounded by pleochroic halos. At the same time, zonation is sometimes observed in zircon crystals, reflecting the multi-stage nature of their formation (Fig. 2f).

The granulite complex of the Kama-Vyatka zone of the Volga-Ural segment was studied using a typical basement section exposed by the Prikazanskaya well 143 in the interval 1826.9–1829.1 m (2.2 m). The rocks of the selected sample for the study (hereinafter Pr 143-1) represent homogeneous slightly gneissic enderbites. The rock structure is hypidiomorphic granular, with elements of lepidogranoblastic texture in thin zones of blastocataclastic transformations. Rock-forming minerals are represented by plagioclase (45–50 vol. %), quartz (30–35 vol. %), orthopyroxene (10–15 vol. %), biotite (5–10 vol. %), hornblende (up to 5 vol. %), potassium feldspar. Accessory and ore minerals: apatite, zircon, magnetite (Fig. 3a).

Plagioclase is evenly distributed in the rock, forming grains of 0.05–1.5 mm in size, with average values of 0.5–0.9 mm. Plagioclase is represented by two varieties – An 34 (andesine) and An 27 (oligoclase). Andesine predominates in the rock, forms larger grains of hypidiomorphic outlines, usually including small antiperthitic intergrowths (Fig. 3b). As a result of blastocataclastic transformations, the grains are partially deformed, which is expressed in the smooth bending of polysynthetic twins. Oligoclase is represented by undeformed isometric grains of smaller size without antiperthitic intergrowths, and is confined to zones of blastocataclasis.

Quartz in the form of xenomorphic grains (up to 2 mm) is concentrated in zones of irregular configuration, showing features of silicification in relation to the early generation plagioclase. In addition, small-grained (up to 0.05 mm) clusters of deformed grains develop in blastocataclasis zones.

Hypersthene is represented by two generations – larger grains (0.5–1.2 mm), possibly of magmatic nature, and surrounding clusters of small (0.02–0.07 mm) grains formed as a result of blastocataclastic transformations (Fig. 3c).

Biotite (up to 0.7 mm) in association with amphibole (up to 0.8 mm) apparently forms during the transformation of first-generation orthopyroxene as a result of superimposed metamorphic processes.

Zircon grains observed during microscopic studies occur as inclusions in first-generation plagioclase or in interstices. They often have distinctly expressed zonal structure of various ranks (Fig. 3d).

### *Research methods*

Analytical studies of the Sm–Nd isotope system of rock samples (quartz diorites TB 238–4 and weakly gneissic enderbites Pr 143-1) were performed on a TRITON mass spectrometer (GEOKHI RAS), the methodology is detailed in (Revyako et al., 2012). The reproducibility of measurements was controlled using the international standard JNdi-1 (Tanaka et al., 2000).

From a sample of quartz diorites TB 238–4 and a sample of weakly gneissic enderbites Pr 143-1, accessory zircon was extracted at the IPGG RAS using a standard methodology based on magnetic separation and heavy liquid separation. The zircon mineral fraction was studied under a Zeiss Stemi 2000-C binocular microscope, the crystals were mounted in a standard 25 mm epoxy resin puck, ground and then the surface polished. To determine the parts of crystals suitable for analysis, zircon grains were first studied using an electron microscope: JEOL JSM 6610 LV (Gubkin Russian State University of Oil and Gas) in cathodoluminescence (CL) mode.

Studies of the U–Pb isotopic system of zircon by LA-ICP-MS were carried out on an ELEMENT XR mass spectrometer with a UP-213 laser attachment (GEOKHI RAS) according to the methodology described in (Kostitsyn, Anosova, 2013). Zircon GJ (Jackson et al., 2004) and 91500 (Wiedenbeck et al., 1995) were used as standards. Based on the measurement results in this work, we obtained a concordant age value for the 91500 zircon standard: 1058 ± 5 million years, MSWD concordance: 2. The obtained data were processed using the Glitter program (van Achterbergh et al., 1999). The Isoplot 4.15 program (Ludwig, 2008) was used to interpret the obtained data and construct diagrams.

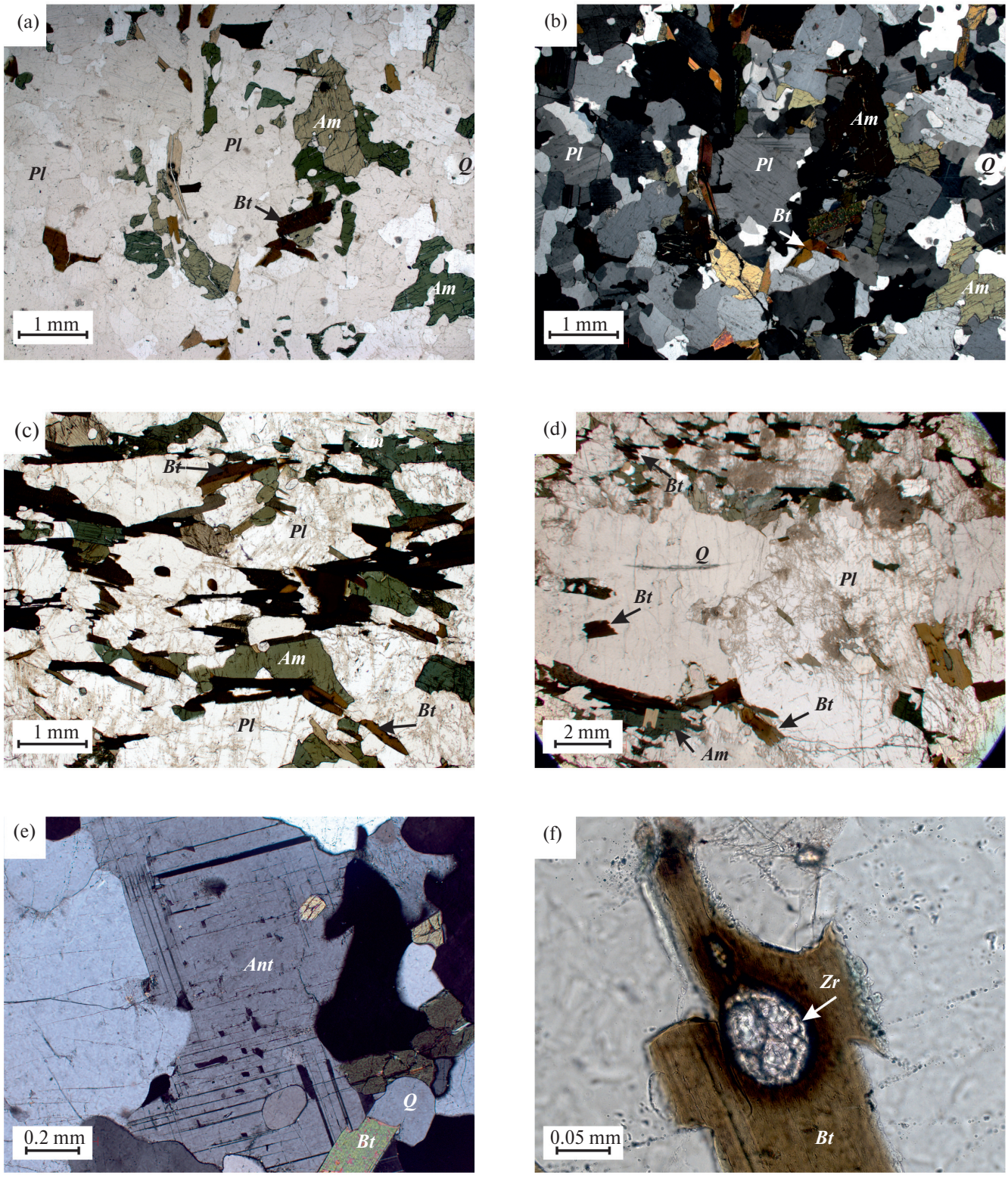


**Fig. 2.** Petrographic features of rocks from the Tanai plagiogranitoid massif of the Kama-Vyatka zone of the Volga-Ural segment: a) quartz diorite, Tanai-Bekhterev well 238, view without analyzer; b) quartz diorite, Tanai-Bekhterev well 238, view with analyzer; c) biotite-amphibole gneiss, gneiss texture, Tanai-Bekhterev well 238, view without analyzer; d) plagiogranite composition veinlet, Tanai-Bekhterev well 238, view without analyzer; e) antiperthitic structure of the inner part of plagioclase grain, Tanai-Bekhterev well 238, view with analyzer; f) newly formed rim around zircon grains of early generation in biotite, Tanai-Bekhterev well 238, view without analyzer.
*Am* – amphibole, *Ant* – antiperthite, *Bt* – biotite, *Pl* – plagioclase, *Q* – quartz, *Zr* – zircon.

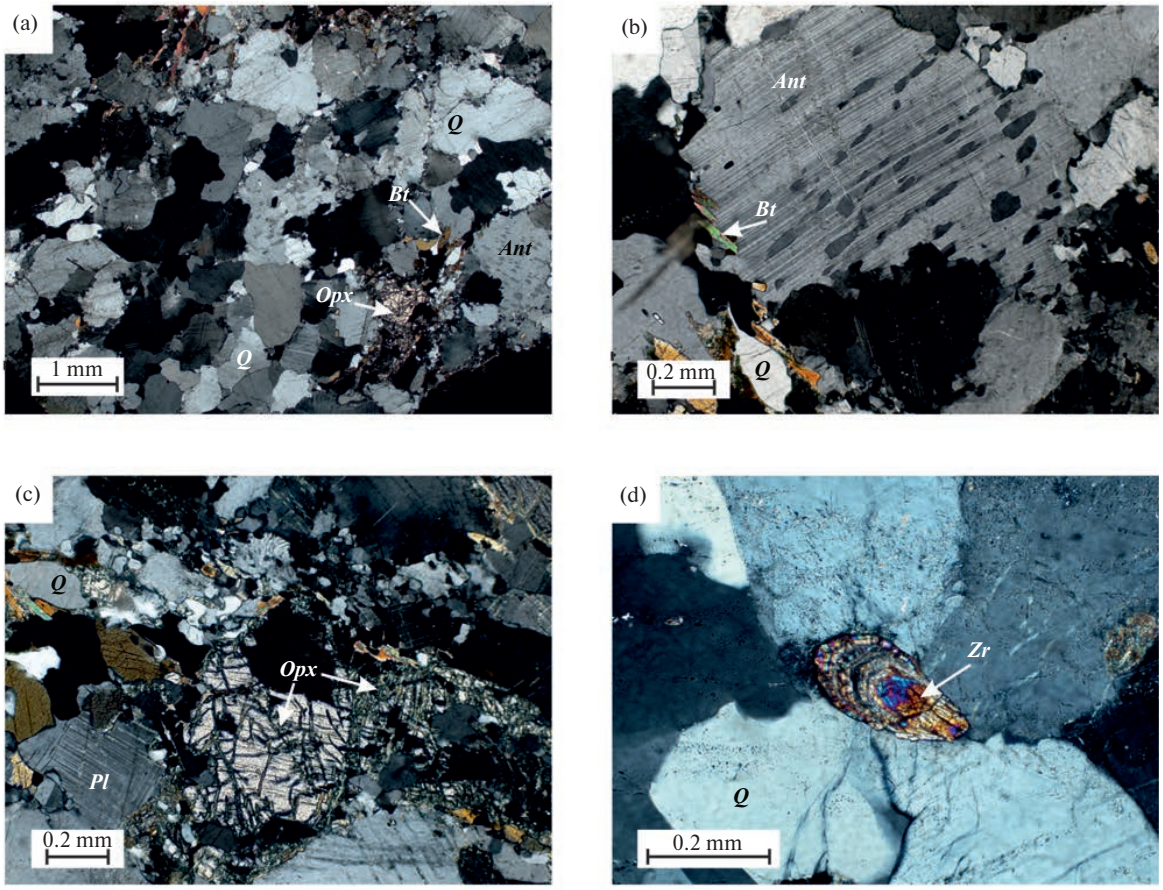


**Fig. 3.** Petrographic features of enderbites from the granulite complex of the Kama-Vyatka zone of the Volga-Ural segment: a) weakly gneissic enderbite, Prikazanskaya well 143, view with analyzer; b) first-generation plagioclase with antiperthitic inclusions, noticeable smooth bending of twins, Prikazanskaya well 143, view with analyzer; c) first-generation hypersthene in the blastocataclasis zone, Prikazanskaya well 143, view with analyzer; d) zonal directional growth of zircon, Prikazanskaya well 143, view with analyzer.
*Ant* – antiperthite, *Bt* – biotite, *Opx* – orthopyroxene, *Pl* – plagioclase, *Q* – quartz, *Zr* – zircon.

Detailed images of zircon for studying the internal structure of crystals were obtained at the second stage on a TESCAN MIRA 3 electron microscope (GEOKHI RAS) in cathodoluminescence (CL) mode at an accelerating voltage of 20 kV.

## RESULTS

**Results of the Sm–Nd isotopic system study of** rock samples, characterizing the main structural-material complexes of the Kama-Vyatka zone, are presented in Table 1. The calculated model ages of quartz diorites of the Tanai plagiogranitoid massif and weakly gneissic enderbites of the Otradnenskaya series were 3.2 and 3.0, respectively. The isotopic composition of Nd in the studied rocks shows that the protolith could have formed due to the reworking of Mesoarchean crust or through mixing of juvenile Mesoarchean material with the addition of Paleoarchean crustal matter. The obtained values of $^{147}Sm/^{144}Nd$ (Table 1) are lower compared to the average crustal values (Taylor, McLennan, 1988; Taylor, McLennan, 2009; Chauvel et al., 2014), which is more consistent with the second assumption.

**Zircon from the quartz diorite sample TB 238-4** is represented by isometric, sometimes slightly elongated ellipsoidal grains; prismatic crystals are less common, and short-prismatic habit crystals are rare. The elongation coefficient of grains ranges from 1:1 to 1:3. The edges and faces of zircon crystals are smoothed. The grains are fractured. In approximately one-third of the grains, the central part (core) and shells of several generations are clearly distinguished. The most representative crystals suitable for geochronological analysis were selected and mounted in a mount in the quantity of 136 pieces. Cathodoluminescence examination was performed for all these crystals (see. Appendix 1, showing images

**Table 1.** Results of Sm–Nd isotopic study of samples of quartz diorites TB 238-4 from the Tanai plagiogranitoid massif and Pr 143-1 – weakly gneissic enderbites of the Otradnensky series

| Sample | Rock | [Sm], ppm | [Nd], ppm | $^{147}Sm/^{144}Nd$ | $^{143}Nd/^{144}Nd$ | ±2σ | $T_{Nd}$, Ga |
|---|---|---|---|---|---|---|---|
| TB 238-4 | quartz diorites | 5.06 | 32.58 | 0.0939 | 0.510634 | 0.000004 | 3.2 |
| Pr 143-1 | enderbites | 6.53 | 37.64 | 0.1049 | 0.510954 | 0.000004 | 3.0 |

Notes. [1]The average value based on the results of measuring the isotopic composition of JNdi-1 during the study period was $^{143}Nd/^{144}Nd = 0.512113 \pm 4$ (2σ, N = 11). The error in determining $^{147}Sm/^{144}Nd$ does not exceed 0.1%.
[2] Model parameters: mantle reservoir (convecting mantle) $^{143}Nd/^{144}Nd = 0.513099$, $^{147}Sm/^{144}Nd = 0.212$. $T_{Nd}$ – model age.

of zircon crystals in secondary electrons (SE) and cathodoluminescence (CL). Circles in the figures indicate craters at LA-ICP-MS analysis points). Based on the internal structure and zonation of the cores, several types of zircon grains are distinguished, images of the most characteristic ones are presented in Fig. 4.

The first type of grains has cores with longitudinal-parallel zonation characteristic of diorites, gabbro-diorites, and more basic rocks (Fig. 4a, b, c, d). In such cores, the faces of the prism, acute and obtuse bipyramids are clearly distinguishable (Fig. 4a, c). In general, these are the most elongated grains with $C_{elong}$ = 1:2–1:3. The number of such grains in the sample is 5–7%.

Some grains of this type have a well-defined shell, with a thickness of up to 20–40 μm (Fig. 4a, c). The shell has gray and light gray cathodoluminescence tones and a distinct block structure. Such a structure is characteristic of zircon formed under conditions of high-temperature metamorphism (Kaulina, 2010). Probably, such a shell is syngenetic to the cores of the third type of grains described below.

The second type of grains has cores with two distinctly discernible growth zones - inner and outer (Fig. 4e, g, i, j). In some grains, only one of these growth zones is visible (Fig. 4f). The inner growth zones of the cores appear homogeneous, dark gray in cathodoluminescence images. In shape, the inner zones of the cores correspond to a combination of prism and obtuse bipyramid. The regular crystallographic forms indicate free crystal growth in the melt. The medium and low intensity of cathodoluminescence (dark gray tones) indicates a relatively high uranium content in the inner zones of zircon cores compared to the outer ones.

The outer growth zones of the cores have a distinct oscillatory zonation and lighter tones. The oscillatory zonation follows the contours of the inner core, but in some cases emphasizes asymmetric growth. This may be a consequence of crystallization under constrained conditions, for example, in a melt with a high percentage of crystalline phase. The lighter CL shade compared to the inner growth zones of zircon indicates a relative decrease in uranium content in the melt during zircon growth (for example, Fig. 4i, Table 2: 238-4-09a, 238-4-09b). Grains with cores of this type typically have an isometric shape – $C_{elong}$ = 1:1–1:2 and make up about 50% of the sample.

Slightly more than one-third of the second type grains have shells (overgrowths) of two generations. The first-generation shells are thin – up to 10 μm thick, discontinuous, with irregular outer boundaries (Fig. 4g, j, k, l). They have light to white tones in cathodoluminescence, indicating relatively low uranium content and, probably, the absence or small amount of water-containing fluid at the time of their crystallization. This, in turn, is characteristic of granulite facies metamorphism (Kaulina, 2010; Rubatto et al., 2001).

The second-generation shells are up to 25 μm thick, dark gray in cathodoluminescence, homogeneous in internal structure or with indistinct zonation (Fig. 4h, k). The saturated gray color indicates a relatively high uranium content and the presence of aqueous fluid, which is characteristic of the amphibolite stage of metamorphism (Rubatto et al., 2001).

The third type of grains has cores with pronounced sectorial zonation and zigzag boundaries between sectors of the "fir-tree" type (Fig. 4m, n, o, p), which is characteristic of zircon formed during metamorphism under granulite facies conditions (Harley et al., 2007). The arrangement of growth sectors within the cores is radial (Fig. 4m, n, p) or chaotic, "patchwork" (Fig. 4 k, o). The crystallization center in some cases is shifted to the edge of the metamorphic cores, demonstrating asymmetry, which also indicates constrained conditions of crystal growth, like the outer growth zone of the second type grain cores. The shape of grains of this type is usually isometric, $C_{elong}$ = 1:1. Their quantity comprises up to 40% of the sample.

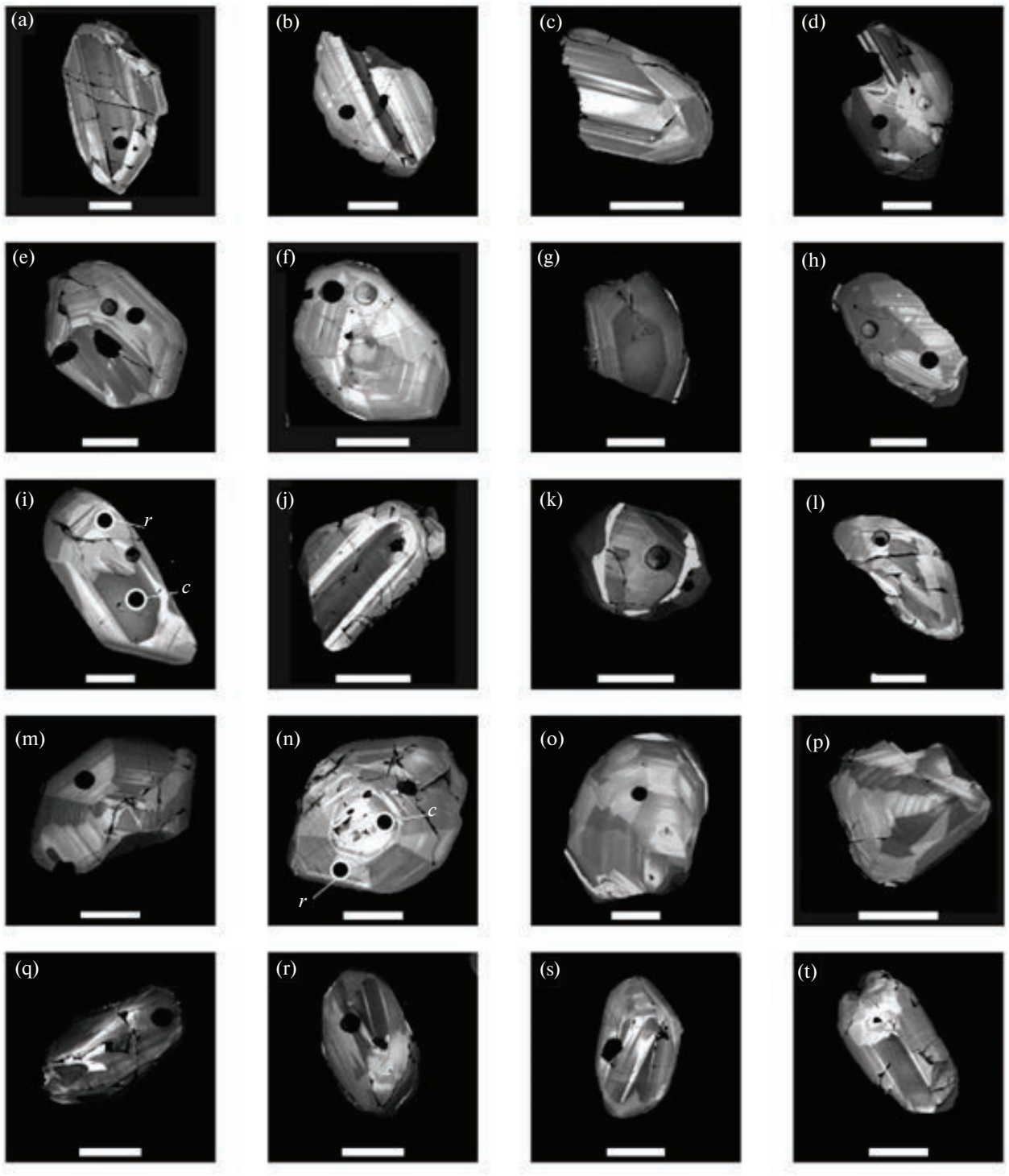


**Fig. 4.** Cathodoluminescence images of typical zircon grains from the quartz diorite sample TB 238-4 of the Tanay plagiogranitoid massif
a–d – zircons with first-type cores having longitudinal-parallel zonation characteristic of gabbroids and gabbro-diorites; e–l – zircons with second-type cores having oscillatory zonation characteristic of granitoids and indicating crystallization from melt. Some crystals have clearly defined inner and outer cores (e, g, i, j). Crystal (l) bears traces of brittle granoblastic deformations; m–p – zircons with third-type cores possessing sectorial zonation and "fir-tree" type boundaries characteristic of granulite facies metamorphism; q–t – zircons with completely recrystallized fourth-type cores, whose primary nature has been completely erased. Latin letters "c" – core, "r" – rim. Scale bar is 100 μm.

**Table 2.** Results of U-Pb isotopic studies of zircon grains from quartz diorites sample TB 238-4 of the Tanai plagiogranitoid massif obtained by LA-ICP-MS method

| Analysis number | Isotope ratios | | | | | | Rho | Content, μg/g | | Th/U | Age, Ma | | D, % |
|---|---|---|---|---|---|---|---|---|---|---|---|---|---|
| | $^{207}Pb/^{206}Pb$ | ±1σ | $^{207}Pb/^{235}U$ | ±1σ | $^{206}Pb/^{238}U$ | ±1σ | | Th | U | | by $^{207}Pb/^{206}Pb$ | ±2σ | |
| 238-4-01 | 0.227 | 0.002 | 18.83 | 0.19 | 0.602 | 0.006 | 0.65 | 80 | 85 | 0.9 | 3 029 | 33 | 0.3 |
| 238-4-02 | 0.226 | 0.003 | 18.46 | 0.21 | 0.593 | 0.006 | 0.66 | 89 | 91 | 1.0 | 3 022 | 36 | –0.6 |
| 238-4-03 | 0.225 | 0.002 | 16.37 | 0.16 | 0.527 | 0.005 | 0.65 | 138 | 115 | 1.2 | 3 020 | 34 | –9.7 |
| 238-4-04 | 0.226 | 0.002 | 19.46 | 0.19 | 0.623 | 0.006 | 0.65 | 87 | 86 | 1.0 | 3 027 | 33 | 3.2 |
| 238-4-06 | 0.226 | 0.002 | 19.05 | 0.19 | 0.610 | 0.006 | 0.65 | 50 | 76 | 0.7 | 3 027 | 34 | 1.5 |
| 238-4-08a | 0.226 | 0.002 | 17.29 | 0.17 | 0.556 | 0.005 | 0.65 | 72 | 85 | 0.9 | 3 020 | 34 | –5.6 |
| 238-4-08b | 0.228 | 0.002 | 19.16 | 0.19 | 0.609 | 0.006 | 0.65 | 45 | 62 | 0.7 | 3 040 | 34 | 0.8 |
| 238-4-09a | 0.225 | 0.002 | 18.34 | 0.18 | 0.591 | 0.006 | 0.65 | 189 | 161 | 1.2 | 3 017 | 34 | –0.8 |
| 238-4-09b | 0.227 | 0.002 | 18.90 | 0.19 | 0.604 | 0.006 | 0.65 | 51 | 61 | 0.8 | 3 030 | 34 | 0.6 |
| 238-4-10 | 0.220 | 0.002 | 17.61 | 0.19 | 0.580 | 0.006 | 0.65 | 133 | 130 | 1.0 | 2 981 | 35 | –1.1 |
| 238-4-11 | 0.224 | 0.002 | 18.43 | 0.19 | 0.597 | 0.006 | 0.65 | 40 | 61 | 0.7 | 3 010 | 35 | 0.2 |
| 238-4-12 | 0.224 | 0.003 | 18.31 | 0.24 | 0.593 | 0.006 | 0.65 | 49 | 83 | 0.6 | 3 010 | 41 | –0.3 |
| 238-4-13 | 0.224 | 0.002 | 18.31 | 0.19 | 0.592 | 0.006 | 0.65 | 69 | 95 | 0.7 | 3 011 | 35 | –0.4 |
| 238-4-14 | 0.226 | 0.002 | 18.53 | 0.19 | 0.594 | 0.006 | 0.65 | 59 | 76 | 0.8 | 3 025 | 35 | –0.6 |
| 238-4-15 | 0.223 | 0.002 | 18.48 | 0.18 | 0.600 | 0.006 | 0.65 | 46 | 68 | 0.7 | 3 006 | 33 | 0.8 |
| 238-4-16 | 0.223 | 0.002 | 18.10 | 0.18 | 0.590 | 0.006 | 0.65 | 65 | 75 | 0.9 | 3 000 | 33 | –0.4 |
| 238-4-18a | 0.224 | 0.002 | 17.69 | 0.17 | 0.572 | 0.005 | 0.65 | 111 | 113 | 1.0 | 3 011 | 33 | –3.1 |
| 238-4-18b | 0.225 | 0.002 | 19.06 | 0.19 | 0.613 | 0.006 | 0.65 | 77 | 85 | 0.9 | 3 019 | 33 | 2.1 |
| 238-4-19 | 0.225 | 0.002 | 18.36 | 0.18 | 0.593 | 0.006 | 0.65 | 51 | 64 | 0.8 | 3 013 | 34 | –0.4 |
| 238-4-20 | 0.225 | 0.002 | 18.15 | 0.18 | 0.586 | 0.006 | 0.65 | 54 | 72 | 0.8 | 3 015 | 33 | –1.4 |
| 238-4-21 | 0.224 | 0.002 | 18.36 | 0.18 | 0.593 | 0.006 | 0.65 | 48 | 60 | 0.8 | 3 013 | 34 | –0.3 |
| 238-4-22 | 0.225 | 0.002 | 16.80 | 0.17 | 0.541 | 0.005 | 0.65 | 95 | 114 | 0.8 | 3 018 | 33 | –7.6 |
| 238-4-23 | 0.225 | 0.003 | 18.49 | 0.21 | 0.597 | 0.006 | 0.65 | 58 | 96 | 0.6 | 3 013 | 37 | 0.2 |
| 238-4-24 | 0.224 | 0.002 | 18.80 | 0.19 | 0.608 | 0.006 | 0.65 | 47 | 60 | 0.8 | 3 011 | 34 | 1.7 |
| 238-4-25 | 0.222 | 0.002 | 18.36 | 0.18 | 0.599 | 0.006 | 0.65 | 64 | 79 | 0.8 | 2 998 | 34 | 0.9 |
| 238-4-27 | 0.224 | 0.002 | 18.54 | 0.19 | 0.599 | 0.006 | 0.65 | 86 | 89 | 1.0 | 3 013 | 34 | 0.5 |
| 238-4-29 | 0.222 | 0.002 | 18.03 | 0.18 | 0.589 | 0.006 | 0.65 | 97 | 100 | 1.0 | 2 994 | 34 | –0.3 |

**Table 2.** (End)

| Analysis number | Isotope ratios | | | | | | Rho | Content, μg/g | | Th/U | Age, Ma | | D, % |
|---|---|---|---|---|---|---|---|---|---|---|---|---|---|
| | $\frac{^{207}Pb}{^{206}Pb}$ | ±1σ | $\frac{^{207}Pb}{^{235}U}$ | ±1σ | $\frac{^{206}Pb}{^{238}U}$ | ±1σ | | Th | U | | by $\frac{^{207}Pb}{^{206}Pb}$ | ±2σ | |
| 238-4-30 | 0.224 | 0.002 | 18.46 | 0.19 | 0.599 | 0.006 | 0.65 | 95 | 92 | 1.0 | 3 007 | 34 | 0.6 |
| 238-4-31 | 0.222 | 0.002 | 18.48 | 0.18 | 0.603 | 0.006 | 0.65 | 69 | 84 | 0.8 | 2 997 | 33 | 1.5 |
| 238-4-32 | 0.225 | 0.002 | 18.78 | 0.18 | 0.605 | 0.006 | 0.65 | 50 | 64 | 0.8 | 3 018 | 33 | 1.1 |
| 238-4-33 | 0.186 | 0.002 | 4.36 | 0.05 | 0.170 | 0.002 | 0.66 | 98 | 365 | 0.3 | 2 708 | 38 | –63 |
| 238-4-34 | 0.221 | 0.002 | 17.88 | 0.19 | 0.588 | 0.006 | 0.66 | 67 | 91 | 0.7 | 2 985 | 34 | –0.2 |
| 238-4-35 | 0.225 | 0.002 | 18.44 | 0.19 | 0.595 | 0.006 | 0.66 | 122 | 115 | 1.1 | 3 015 | 34 | –0.1 |
| 238-4-38 | 0.225 | 0.002 | 18.71 | 0.18 | 0.604 | 0.006 | 0.65 | 146 | 152 | 1.0 | 3 014 | 33 | 1.1 |
| 238-4-39 | 0.224 | 0.002 | 18.47 | 0.18 | 0.599 | 0.006 | 0.65 | 71 | 90 | 0.8 | 3 007 | 33 | 0.6 |
| 238-4-40 | 0.223 | 0.002 | 18.36 | 0.18 | 0.598 | 0.006 | 0.65 | 107 | 138 | 0.8 | 3 000 | 33 | 0.8 |
| 238-4-41 | 0.225 | 0.002 | 18.47 | 0.18 | 0.596 | 0.006 | 0.65 | 65 | 81 | 0.8 | 3 015 | 34 | 0.0 |
| 238-4-42 | 0.221 | 0.002 | 17.95 | 0.18 | 0.589 | 0.006 | 0.65 | 78 | 112 | 0.7 | 2 987 | 34 | 0.0 |
| 238-4-43 | 0.161 | 0.002 | 9.31 | 0.11 | 0.419 | 0.005 | 0.66 | 62 | 172 | 0.4 | 2 469 | 40 | –8.7 |
| 238-4-44 | 0.222 | 0.002 | 18.16 | 0.18 | 0.593 | 0.006 | 0.65 | 51 | 70 | 0.7 | 2 996 | 34 | 0.2 |
| 238-4-45 | 0.225 | 0.002 | 18.81 | 0.19 | 0.607 | 0.006 | 0.65 | 63 | 78 | 0.8 | 3 014 | 34 | 1.5 |
| 238-4-48 | 0.223 | 0.002 | 18.64 | 0.20 | 0.605 | 0.006 | 0.65 | 52 | 74 | 0.7 | 3 005 | 35 | 1.5 |
| 238-4-49 | 0.224 | 0.002 | 17.66 | 0.18 | 0.572 | 0.005 | 0.65 | 100 | 104 | 1.0 | 3 009 | 34 | –3.1 |
| 238-4-50 | 0.223 | 0.002 | 17.99 | 0.18 | 0.586 | 0.006 | 0.65 | 79 | 93 | 0.8 | 2 999 | 35 | –0.8 |
| 238-4-50b | 0.226 | 0.003 | 17.38 | 0.22 | 0.558 | 0.006 | 0.66 | 87 | 99 | 0.9 | 3 023 | 39 | –5.4 |
| 238-4-51 | 0.193 | 0.002 | 8.03 | 0.10 | 0.302 | 0.003 | 0.65 | 296 | 403 | 0.7 | 2 768 | 41 | –39 |
| 238-4-52 | 0.167 | 0.002 | 7.86 | 0.10 | 0.342 | 0.004 | 0.66 | 122 | 460 | 0.3 | 2 525 | 41 | –25 |
| 238-4-54 | 0.192 | 0.002 | 8.60 | 0.11 | 0.325 | 0.003 | 0.66 | 367 | 416 | 0.9 | 2 758 | 40 | –34 |
| 238-4-57 | 0.213 | 0.003 | 5.97 | 0.08 | 0.204 | 0.002 | 0.64 | 63 | 149 | 0.4 | 2 925 | 45 | –59 |
| 238-4-60 | 0.228 | 0.003 | 18.59 | 0.24 | 0.593 | 0.006 | 0.66 | 162 | 180 | 0.9 | 3 035 | 40 | –1.2 |
| 238-4-68 | 0.218 | 0.003 | 15.90 | 0.23 | 0.529 | 0.006 | 0.65 | 550 | 396 | 1.4 | 2 966 | 44 | –7.7 |
| 238-4-70 | 0.181 | 0.002 | 11.78 | 0.16 | 0.472 | 0.005 | 0.65 | 161 | 393 | 0.4 | 2 662 | 43 | –6.4 |
| 238-4-71 | 0.228 | 0.003 | 18.63 | 0.24 | 0.594 | 0.007 | 0.65 | 86 | 90 | 1.0 | 3 035 | 41 | –1.0 |
| 238-4-73 | 0.216 | 0.003 | 15.80 | 0.22 | 0.532 | 0.006 | 0.65 | 186 | 203 | 0.9 | 2 948 | 43 | –6.8 |

Notes. Rho – error correlation coefficient $^{207}Pb/^{235}U$ – $^{206}Pb/^{238}U$, D – degree of discordance: (((age by $^{206}Pb/^{238}U$)/(age by $^{207}Pb/^{206}Pb$)) – 1)*100.

Individual grains of the third type (for example, Fig. 4o) have shells (overgrowths) of two generations, similar to those in the second type grains described above (see Fig. 4g, j, k, l and Fig. 4 h, k, respectively). Their thickness is extremely small and does not exceed 10 μm. The contours of the shells are distinctly discordant with the internal sectorial structure of the metamorphic cores and cut across it, indicating their formation in a separate crystallization process.

In some cases, sectorial – "granulite" – zoning overlaps with longitudinal-parallel zoning in grains of the first type (Fig. 4d) and oscillatory zoning of grains of the second type (Fig. 4f, h, l), partially obscuring the primary structure of zircon cores. The extreme manifestation of such a process can be considered as completely recrystallized cores of grains of the fourth type (Fig. 4q, r, s, t), for which it is impossible to restore the primary zoning. Their quantity in the sample does not exceed 5%. Some grains show signs of brittle deformations (for example, Fig. 4m).

The rims in grains of the fourth type are represented by fragmentary, discontinuous overgrowths up to 10 μm thick, of gray and dark gray shades in cathodoluminescent images (Fig. 4r, t). They are probably identical to the "amphibolite" rims of the second generation on grains of the second and third types.

**Investigations of the U–Pb isotopic system of zircon**. Using the LA-ICP-MS method, 50 zircon grains from the quartz diorite sample TB 238-4 were analyzed; in 4 zircon crystals, analysis was performed at two points – central part-rim (Fig. 5a, Table 2 (numbers in the table correspond to the point numbers presented in Appendix 1). U contents range from 60 to 460 μg/g, Th – 40–550 μg/g, Th/U ratio – 0.27–1.39. 17 determined values are discordant D > 2%. The obtained ages based on the isotopic ratio $^{207}Pb/^{206}Pb$ with D ⩽ 2% range from 3.04–2.98 billion years (Fig. 5a (inset), 5b).

**Zircon grains isolated from the sample of weakly gneissic enderbites Pr 143-1,** have colors ranging from almost transparent with a pinkish-brown tinge to lilac-brownish. Oval-shaped grains with elongation $C_{elong}$ = 1:2–1:3 and without clearly expressed faces predominate. There are single grains of ellipsoidal shape with elongation $C_{elon}g$ = 1:4–1:5, and well-defined prism faces and sharp bipyramid.

No signs of dissolution of internal or external parts of the grains are observed. From this, it can be assumed that the rounded shape of the grains formed due to the formation of granoblastic rock structure during deformations synchronous with metamorphic processes.

172 crystals were selected and mounted in a puck for cathodoluminescence and geochronological studies. Fig. 6 shows images of the most characteristic zircon grains.

All zircon grains, regardless of morphology, have a well-defined core and one or two generations of rims (see Appendix 2, which shows images of zircon crystals in secondary electrons (SE) and cathodoluminescence (CL). The rings in the figures indicate craters at LA-ICP-MS analysis points). The cores in oval grains also have a rounded shape without clearly defined faces. In CL images, they mainly have a uniform gray color. Only a few crystals show vague traces of oscillatory zoning (Fig. 6, grains 1b, 2a, 2c, 3a, 4a), indicating crystallization of zircon from melt and the probable magmatic origin of zircon. Some zircon grains (Fig. 6, grains 1a, 1c, 1d) in CL images have cores with intense light coloration, indicating low uranium content. This is characteristic of zircon formed under granulite facies conditions (Kaulina, 2010; Rubatto et al., 2001). In some cases, the superimposition of sectorial metamorphic zoning on oscillatory magmatic zoning is clearly visible (Fig. 6, grain 1b). This may be a consequence of recrystallization of magmatic zircon in the final stages of its formation under *P–T* conditions of granulite facies.

The earliest overgrowths on zircon cores are represented by dark gray rims in CL images. This indicates relatively high uranium content, which is characteristic of amphibolite facies metamorphism. Apparently, new zircon crystals corresponding to this stage are formed simultaneously, having intensely gray central parts of grains in CL images (Fig. 6, grains 2b, 2c, 2d) – second generation zircon.

Zircon of the next – third generation is represented by relatively thin, very light rims in CL images (Fig. 6, grains 1a, 1c, 1d, 2c, 2d, 3b, 3d, 4a, 4b, 4c, 4d). The light tone indicates low uranium concentrations in such rims. In some cases, one can see an indistinct sectorial structure of newly formed rims with zigzag boundaries of the "fir-tree" type, which is characteristic of zircon crystallized under granulite facies metamorphism conditions (Fig. 6, grains 1a, 2b, 2d, 4b).

The latest overgrowths are represented predominantly by dark CL images and, consequently, high-uranium thin shells (Fig. 6, grain 4d). In some cases, recrystallization of zircon cores from previous generations occurs. Fig. 6 (grains 4a, 4b, 4c, 4d) shows zircon grains with cores recrystallized in amphibolite facies.

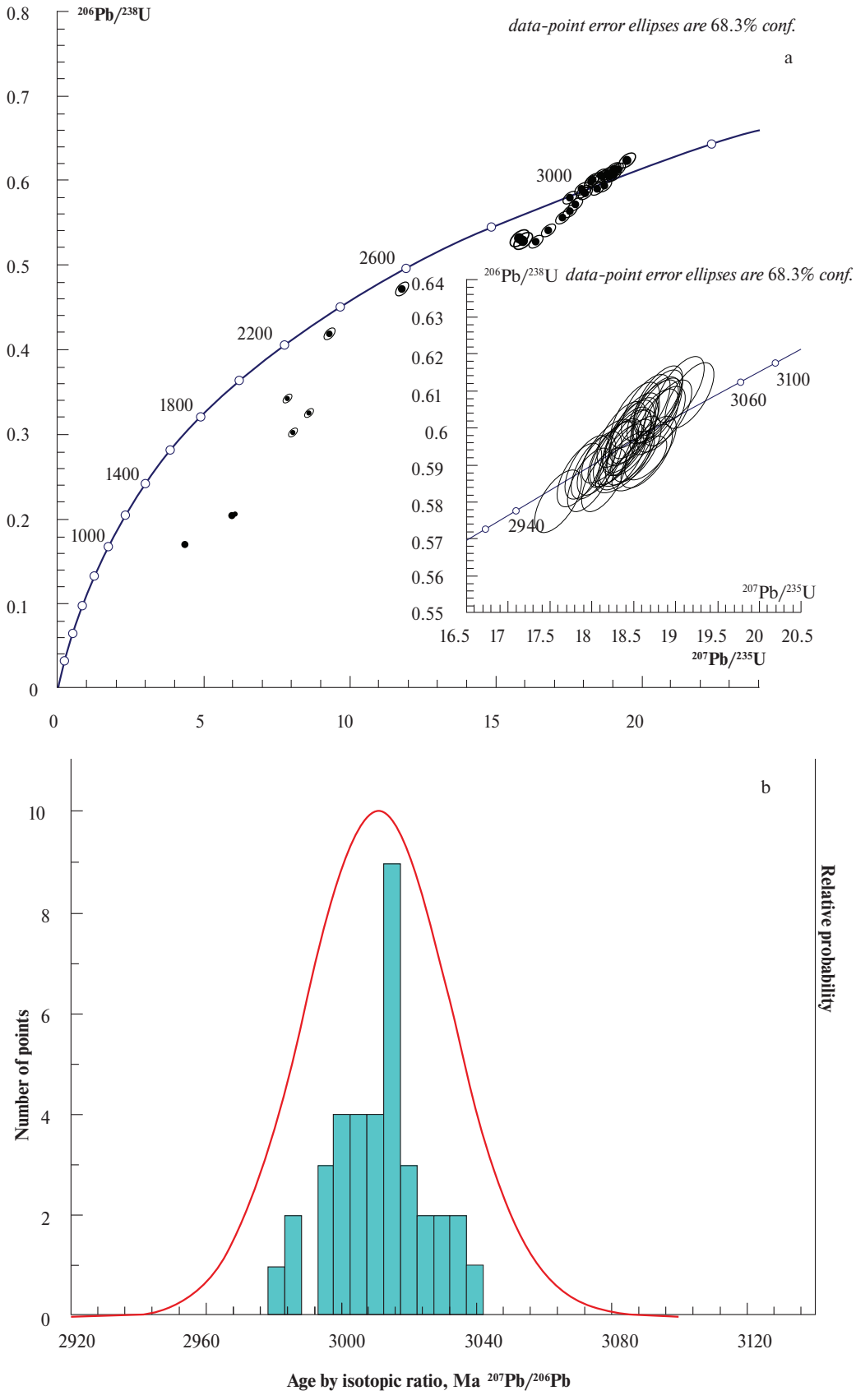


**Fig. 5.** a) Concordia diagram for zircon from quartz diorite sample TB 238-4 of the Tanai plagiogranitoid massif (inset: points with D ⩽ 2%); b) histogram and distribution of relative age probabilities according to the isotopic ratio $^{207}Pb/^{206}Pb$ (D ⩽ 2%).

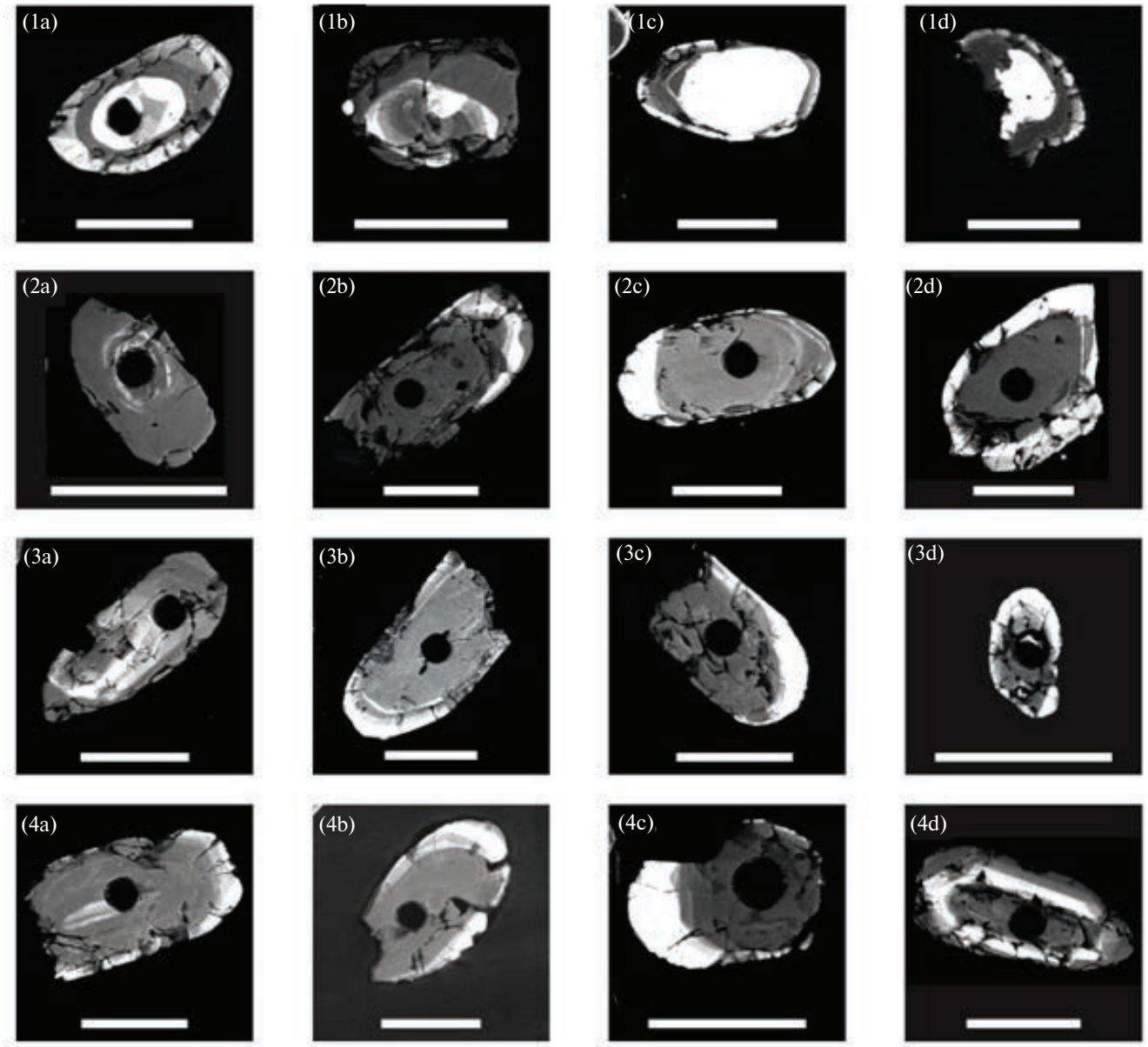


**Fig. 6.** Cathodoluminescence images of typical zircon grains from the sample of weakly gneissic enderbites Pr 143-1 of the Otradnensky series of the Kama-Vyatka zone.
1a–d – zircons with ancient cores of the earliest – first generation, formed in a magmatic process and recrystallized at the final stages of formation under granulite facies conditions; 2a – the second generation core has shadow oscillatory zoning, indicating the crystallization of this zircon grain from a melt, possibly during partial melting under granulite facies metamorphism conditions; 2b–d – zircons with cores of the third generation, formed during ultrametamorphism under amphibolite facies conditions; 3a–d – zircons with cores and shells of the fourth generation, formed under granulite facies metamorphism conditions; 4a–d – zircons with recrystallized cores of the latest – fifth generation. The scale bar is 100 μm.

**U–Pb isotope system studies of zircon**. The U–Pb isotope system of zircon from sample of weakly gneissic enderbites Pr 143-1 was analyzed by LA-ICP-MS in 74 grains; in 12 of these grains, measurements were taken at two points corresponding to different zones of the crystal (Fig. 7a, Table 3 (numbers in the table correspond to point numbers presented in Appendix 2). The histogram and probability density distribution curves of age values based on the isotopic ratio $^{207}Pb/^{206}Pb$ were constructed for 40 points with discordance D < 2% (Fig. 7b). In Fig. 7b, one can see that the obtained age values are distributed in the intervals of 3.0–2.8 and 2.75–2.60 billion years (values calculated from the isotopic ratio $^{207}Pb/^{206}Pb$).

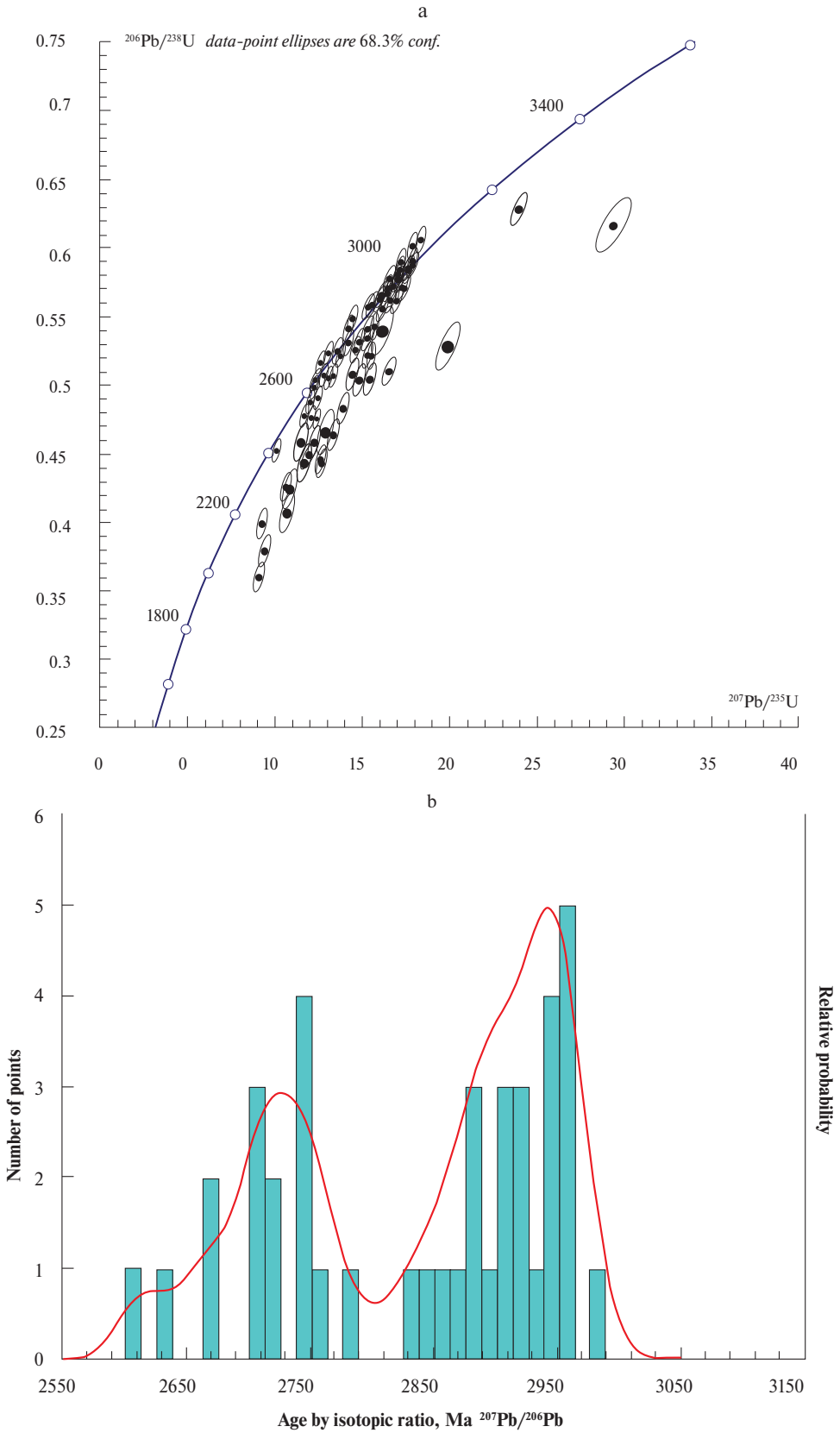


**Fig. 7.** a) Concordia diagram for zircon from sample of slightly gneissic enderbites Pr 143-1,, studied by LA-ICP-MS method. b) Histogram and probability density distribution curve of zircon age values from the sample of slightly gneissic enderbites Pr 143-1, calculated from the isotopic ratio $^{207}Pb/^{206}Pb$, D < 2%.

**Table 3.** Results of U–Pb isotopic studies of zircon grains from sample Pr 143-1 of weakly gneissic enderbites of the Otradnenskaya series, obtained by LA-ICP-MS

| Analysis number | Isotope ratios | | | | | | Rho | Content, μg/g | | Th/U | Age, Ma | | D, % |
|---|---|---|---|---|---|---|---|---|---|---|---|---|---|
| | $\frac{^{207}Pb}{^{206}Pb}$ | ±1σ | $\frac{^{207}Pb}{^{235}U}$ | ±1σ | $\frac{^{206}Pb}{^{238}U}$ | ±1σ | | Th | U | | by $\frac{^{207}Pb}{^{206}Pb}$ | ±2σ | |
| 143-1-line5-02 | 0.208 | 0.002 | 15.98 | 0.18 | 0.559 | 0.006 | 0.66 | 73 | 546 | 0.134 | 2 886 | 36 | –0.9 |
| 143-1-line5-03 | 0.210 | 0.002 | 16.37 | 0.18 | 0.566 | 0.006 | 0.67 | 184 | 701 | 0.263 | 2 903 | 35 | –0.4 |
| 143-1-line5-04 | 0.186 | 0.002 | 13.11 | 0.16 | 0.511 | 0.006 | 0.67 | 30 | 2014 | 0.015 | 2 707 | 37 | –1.7 |
| 143-1-line5-05 | 0.211 | 0.002 | 15.74 | 0.19 | 0.540 | 0.006 | 0.66 | 160 | 1423 | 0.112 | 2 915 | 38 | –4.5 |
| 143-1-line5-06b | 0.188 | 0.002 | 12.35 | 0.14 | 0.476 | 0.005 | 0.66 | 86 | 804 | 0.107 | 2 727 | 38 | –8.0 |
| 143-1-line5-06c | 0.206 | 0.002 | 15.99 | 0.18 | 0.564 | 0.006 | 0.66 | 331 | 3302 | 0.100 | 2 871 | 36 | 0.4 |
| 143-1-line5-07b | 0.212 | 0.002 | 17.12 | 0.21 | 0.584 | 0.007 | 0.68 | 165 | 513 | 0.321 | 2 924 | 35 | 1.5 |
| 143-1-line5-07c | 0.211 | 0.002 | 17.15 | 0.21 | 0.590 | 0.007 | 0.69 | 271 | 676 | 0.401 | 2 910 | 35 | 2.8 |
| 143-1-line5-08 | 0.205 | 0.002 | 15.22 | 0.18 | 0.538 | 0.006 | 0.67 | 79 | 421 | 0.187 | 2 867 | 36 | –3.2 |
| 143-1-line5-10b | 0.184 | 0.002 | 12.45 | 0.16 | 0.490 | 0.005 | 0.65 | 99 | 91 | 1.094 | 2 690 | 42 | –4.4 |
| 143-1-line5-10c | 0.202 | 0.003 | 15.45 | 0.21 | 0.555 | 0.006 | 0.65 | 136 | 664 | 0.204 | 2 842 | 42 | 0.1 |
| 143-1-line5-11 | 0.188 | 0.002 | 13.58 | 0.17 | 0.525 | 0.006 | 0.68 | 132 | 138 | 0.960 | 2 722 | 37 | 0.0 |
| 143-1-line5-14 | 0.187 | 0.002 | 13.21 | 0.15 | 0.512 | 0.005 | 0.67 | 42 | 1048 | 0.040 | 2 716 | 36 | –1.8 |
| 143-1-line5-15 | 0.212 | 0.002 | 16.12 | 0.19 | 0.552 | 0.006 | 0.66 | 383 | 2805 | 0.136 | 2 920 | 37 | –3.0 |
| 143-1-line5-16 | 0.182 | 0.002 | 13.09 | 0.15 | 0.523 | 0.006 | 0.66 | 2817 | 16084 | 0.175 | 2 667 | 37 | 1.7 |
| 143-1-line5-17 | 0.191 | 0.002 | 13.33 | 0.15 | 0.506 | 0.005 | 0.67 | 345 | 6503 | 0.053 | 2 750 | 36 | –4.0 |
| 143-1-line5-20 | 0.176 | 0.002 | 12.03 | 0.14 | 0.497 | 0.005 | 0.66 | 233 | 2133 | 0.109 | 2 612 | 38 | –0.4 |
| 143-1-line5-22b | 0.191 | 0.002 | 14.20 | 0.18 | 0.539 | 0.006 | 0.68 | 114 | 152 | 0.747 | 2 750 | 37 | 1.1 |
| 143-1-line5-22c | 0.219 | 0.002 | 18.31 | 0.23 | 0.606 | 0.007 | 0.68 | 260 | 1322 | 0.197 | 2 975 | 36 | 2.6 |
| 143-1-line5-25 | 0.219 | 0.003 | 17.84 | 0.23 | 0.590 | 0.007 | 0.68 | 68 | 115 | 0.588 | 2 976 | 37 | 0.4 |
| 143-1-line5-26b | 0.190 | 0.002 | 14.13 | 0.18 | 0.539 | 0.006 | 0.68 | 124 | 426 | 0.292 | 2 743 | 37 | 1.4 |
| 143-1-line5-26c | 0.215 | 0.002 | 17.78 | 0.22 | 0.600 | 0.007 | 0.68 | 256 | 596 | 0.430 | 2 942 | 37 | 3.1 |
| 143-1-line5-28 | 0.215 | 0.002 | 16.78 | 0.20 | 0.567 | 0.006 | 0.67 | 87 | 383 | 0.226 | 2 940 | 36 | –1.4 |
| 143-1-line5-29 | 0.211 | 0.002 | 16.34 | 0.19 | 0.562 | 0.006 | 0.67 | 105 | 926 | 0.114 | 2 912 | 36 | –1.2 |
| 143-1-line5-30 | 0.216 | 0.003 | 17.00 | 0.21 | 0.571 | 0.006 | 0.67 | 83 | 354 | 0.233 | 2 950 | 38 | –1.3 |
| 143-1-line5-31 | 0.203 | 0.002 | 15.66 | 0.18 | 0.560 | 0.006 | 0.66 | 180 | 1261 | 0.143 | 2 851 | 37 | 0.5 |
| 143-1-line5-32 | 0.216 | 0.002 | 16.91 | 0.20 | 0.569 | 0.006 | 0.67 | 94 | 390 | 0.242 | 2 947 | 36 | –1.5 |
| 143-1-line5-33 | 0.186 | 0.002 | 13.17 | 0.17 | 0.514 | 0.006 | 0.67 | 72 | 1038 | 0.069 | 2 705 | 39 | –1.2 |
| 143-1-line5-34 | 0.187 | 0.002 | 11.58 | 0.15 | 0.449 | 0.005 | 0.66 | 894 | 1127 | 0.793 | 2 717 | 40 | –12 |
| 143-1-line5-35 | 0.208 | 0.002 | 16.54 | 0.20 | 0.578 | 0.006 | 0.66 | 88 | 828 | 0.106 | 2 886 | 39 | 1.9 |
| 143-1-line5-36 | 0.177 | 0.002 | 12.64 | 0.15 | 0.518 | 0.005 | 0.66 | 127 | 3156 | 0.040 | 2 626 | 39 | 2.4 |
| 143-1-line5-37 | 0.277 | 0.004 | 23.98 | 0.32 | 0.628 | 0.007 | 0.65 | 317 | 812 | 0.391 | 3 344 | 41 | –6.0 |
| 143-1-line5-38 | 0.219 | 0.003 | 16.97 | 0.22 | 0.562 | 0.006 | 0.65 | 759 | 656 | 1.156 | 2 972 | 40 | –3.2 |
| 143-1-line5-39 | 0.214 | 0.002 | 16.78 | 0.21 | 0.569 | 0.006 | 0.67 | 129 | 1042 | 0.124 | 2 935 | 37 | –1.1 |
| 143-1-line5-40 | 0.220 | 0.003 | 17.31 | 0.24 | 0.571 | 0.007 | 0.65 | 15 | 38 | 0.398 | 2 980 | 43 | –2.3 |

**Table 3.** (Continued)

| Analysis number | Isotope ratios | | | | | | Rho | Content, μg/g | | Th/U | Age, Ma | | D, % |
|---|---|---|---|---|---|---|---|---|---|---|---|---|---|
| | $\frac{^{207}Pb}{^{206}Pb}$ | ±1σ | $\frac{^{207}Pb}{^{235}U}$ | ±1σ | $\frac{^{206}Pb}{^{238}U}$ | ±1σ | | Th | U | | by $\frac{^{207}Pb}{^{206}Pb}$ | ±2σ | |
| 143-1-line5-42 | 0.200 | 0.003 | 15.37 | 0.21 | 0.557 | 0.006 | 0.64 | 69 | 494 | 0.141 | 2 826 | 44 | 1.0 |
| 143-1-line5-43 | 0.207 | 0.003 | 16.20 | 0.20 | 0.568 | 0.006 | 0.66 | 186 | 1164 | 0.160 | 2 881 | 40 | 0.6 |
| 143-1-line5-44 | 0.208 | 0.002 | 16.12 | 0.20 | 0.563 | 0.006 | 0.67 | 86 | 754 | 0.113 | 2 888 | 39 | –0.3 |
| 143-1-line5-45 | 0.186 | 0.002 | 13.11 | 0.17 | 0.512 | 0.006 | 0.67 | 286 | 145 | 1.974 | 2 705 | 40 | –1.5 |
| 143-1-line5-49 | 0.217 | 0.003 | 17.76 | 0.22 | 0.594 | 0.007 | 0.67 | 100 | 944 | 0.106 | 2 957 | 38 | 1.7 |
| 143-1-line5-49b | 0.162 | 0.003 | 10.11 | 0.16 | 0.452 | 0.006 | 0.65 | 62 | 21 | 2.923 | 2 479 | 52 | –3.0 |
| 143-1-line5-50b | 0.192 | 0.002 | 14.49 | 0.18 | 0.549 | 0.006 | 0.67 | 111 | 491 | 0.226 | 2 756 | 39 | 2.3 |
| 143-1-line5-50c | 0.216 | 0.003 | 17.10 | 0.22 | 0.575 | 0.007 | 0.67 | 135 | 217 | 0.623 | 2 948 | 38 | –0.6 |
| 143-1-line5-54 | 0.217 | 0.003 | 17.26 | 0.23 | 0.577 | 0.007 | 0.67 | 96 | 342 | 0.281 | 2 958 | 40 | –0.7 |
| 143-1-line5-55 | 0.212 | 0.003 | 16.43 | 0.21 | 0.561 | 0.006 | 0.67 | 484 | 704 | 0.688 | 2 923 | 39 | –1.8 |
| 143-1-line6-01 | 0.180 | 0.002 | 12.26 | 0.21 | 0.495 | 0.008 | 0.73 | 79 | 3114 | 0.025 | 2 651 | 41 | –2.3 |
| 143-1-line6-02 | 0.216 | 0.003 | 17.41 | 0.35 | 0.584 | 0.010 | 0.71 | 3843 | 2357 | 1.631 | 2 952 | 48 | 0.4 |
| 143-1-line6-06 | 0.187 | 0.003 | 13.08 | 0.19 | 0.506 | 0.006 | 0.64 | 218 | 125 | 1.751 | 2 720 | 46 | –3.0 |
| 143-1-line6-07 | 0.215 | 0.003 | 17.29 | 0.29 | 0.582 | 0.009 | 0.73 | 79 | 416 | 0.190 | 2 946 | 39 | 0.4 |
| 143-1-line6-08 | 0.213 | 0.003 | 15.16 | 0.27 | 0.517 | 0.009 | 0.73 | 755 | 969 | 0.779 | 2 927 | 42 | –8.2 |
| 143-1-line6-10 | 0.206 | 0.003 | 12.65 | 0.22 | 0.446 | 0.007 | 0.72 | 320 | 710 | 0.451 | 2 873 | 42 | –17 |
| 143-1-line6-12 | 0.211 | 0.003 | 15.04 | 0.26 | 0.518 | 0.008 | 0.73 | 407 | 3291 | 0.124 | 2 910 | 39 | –7.5 |
| 143-1-line6-14b | 0.190 | 0.002 | 13.87 | 0.18 | 0.530 | 0.006 | 0.66 | 171 | 470 | 0.365 | 2 742 | 41 | –0.1 |
| 143-1-line6-14c | 0.212 | 0.003 | 16.71 | 0.21 | 0.573 | 0.006 | 0.66 | 167 | 606 | 0.276 | 2 918 | 39 | 0.1 |
| 143-1-line6-17 | 0.206 | 0.003 | 14.47 | 0.27 | 0.509 | 0.008 | 0.72 | 308 | 2356 | 0.131 | 2 877 | 44 | –7.9 |
| 143-1-line6-17b | 0.191 | 0.002 | 13.77 | 0.18 | 0.522 | 0.006 | 0.65 | 110 | 144 | 0.761 | 2 752 | 42 | –1.5 |
| 143-1-line6-22b | 0.182 | 0.002 | 13.07 | 0.17 | 0.521 | 0.006 | 0.66 | 65 | 1226 | 0.053 | 2 671 | 41 | 1.2 |
| 143-1-line6-22c | 0.195 | 0.002 | 14.27 | 0.19 | 0.531 | 0.006 | 0.65 | 196 | 421 | 0.466 | 2 783 | 41 | –1.3 |
| 143-1-line6-27 | 0.209 | 0.002 | 13.90 | 0.23 | 0.483 | 0.008 | 0.73 | 188 | 668 | 0.282 | 2 894 | 39 | –12 |
| 143-1-line6-28 | 0.222 | 0.003 | 15.43 | 0.27 | 0.505 | 0.008 | 0.73 | 301 | 516 | 0.582 | 2 992 | 40 | –12 |
| 143-1-line6-30 | 0.207 | 0.003 | 12.69 | 0.23 | 0.444 | 0.007 | 0.72 | 823 | 3592 | 0.229 | 2 885 | 43 | –18 |
| 143-1-line6-31 | 0.181 | 0.003 | 10.61 | 0.20 | 0.426 | 0.007 | 0.71 | 930 | 2282 | 0.407 | 2 659 | 48 | –14 |
| 143-1-line6-32 | 0.208 | 0.003 | 13.31 | 0.23 | 0.464 | 0.007 | 0.73 | 982 | 1891 | 0.519 | 2 892 | 39 | –15 |
| 143-1-line6-33 | 0.168 | 0.003 | 9.24 | 0.19 | 0.399 | 0.007 | 0.71 | 2496 | 6854 | 0.364 | 2 537 | 53 | –15 |
| 143-1-line6-34 | 0.194 | 0.003 | 12.27 | 0.24 | 0.459 | 0.008 | 0.72 | 8234 | 5250 | 1.568 | 2 777 | 47 | –12 |
| 143-1-line6-35 | 0.178 | 0.003 | 12.20 | 0.28 | 0.497 | 0.010 | 0.74 | 143 | 2634 | 0.054 | 2 634 | 50 | –1.2 |
| 143-1-line6-36b | 0.183 | 0.003 | 9.10 | 0.22 | 0.361 | 0.008 | 0.75 | 19 | 805 | 0.024 | 2 680 | 50 | –26 |
| 143-1-line6-36c | 0.345 | 0.006 | 29.39 | 0.70 | 0.617 | 0.013 | 0.73 | 484 | 494 | 0.980 | 3 687 | 50 | –16 |
| 143-1-line6-37 | 0.179 | 0.003 | 9.40 | 0.24 | 0.380 | 0.008 | 0.75 | 766 | 1358 | 0.564 | 2 647 | 53 | –22 |
| 143-1-line6-40 | 0.235 | 0.004 | 16.56 | 0.29 | 0.510 | 0.007 | 0.64 | 5 | 14 | 0.356 | 3 088 | 54 | –14 |
| 143-1-line6-41 | 0.217 | 0.003 | 17.55 | 0.23 | 0.586 | 0.006 | 0.66 | 138 | 1231 | 0.112 | 2 962 | 40 | 0.3 |

**Table 3.** (End)

| Analysis number | Isotope ratios | | | | | | Rho | Content, μg/g | | Th/U | Age, Ma | | D, % |
|---|---|---|---|---|---|---|---|---|---|---|---|---|---|
| | $\frac{^{207}Pb}{^{206}Pb}$ | ±1σ | $\frac{^{207}Pb}{^{235}U}$ | ±1σ | $\frac{^{206}Pb}{^{238}U}$ | ±1σ | | Th | U | | by $\frac{^{207}Pb}{^{206}Pb}$ | ±2σ | |
| 143-1-line6-44 | 0.273 | 0.004 | 19.88 | 0.46 | 0.529 | 0.011 | 0.76 | 71 | 574 | 0.123 | 3 320 | 44 | –18 |
| 143-1-line6-45 | 0.192 | 0.003 | 11.78 | 0.28 | 0.445 | 0.010 | 0.76 | 236 | 1627 | 0.145 | 2 760 | 48 | –14 |
| 143-1-line6-46 | 0.191 | 0.003 | 10.68 | 0.27 | 0.406 | 0.009 | 0.75 | 7 | 379 | 0.018 | 2 748 | 53 | –20 |
| 143-1-line6-47 | 0.185 | 0.003 | 10.85 | 0.29 | 0.425 | 0.010 | 0.75 | 223 | 3658 | 0.061 | 2 701 | 57 | –16 |
| 143-1-line6-48 | 0.182 | 0.003 | 11.53 | 0.31 | 0.459 | 0.011 | 0.75 | 98 | 1445 | 0.068 | 2 673 | 55 | –8.9 |
| 143-1-line6-49 | 0.200 | 0.004 | 12.81 | 0.39 | 0.465 | 0.012 | 0.73 | 138 | 2915 | 0.047 | 2 826 | 66 | –13 |
| 143-1-line6-55 | 0.204 | 0.004 | 15.04 | 0.48 | 0.535 | 0.014 | 0.72 | 266 | 584 | 0.455 | 2 858 | 71 | –3.3 |
| 143-1-line6-56 | 0.213 | 0.004 | 15.34 | 0.50 | 0.522 | 0.014 | 0.74 | 132 | 1019 | 0.129 | 2 928 | 68 | –7.5 |
| 143-1-line6-58 | 0.214 | 0.004 | 15.05 | 0.41 | 0.511 | 0.012 | 0.75 | 81 | 368 | 0.219 | 2 934 | 54 | –9.3 |
| 143-1-line6-58b | 0.181 | 0.002 | 11.83 | 0.16 | 0.475 | 0.005 | 0.65 | 60 | 177 | 0.342 | 2 660 | 43 | –5.9 |
| 143-1-line6-59 | 0.217 | 0.004 | 16.22 | 0.46 | 0.542 | 0.013 | 0.76 | 100 | 785 | 0.128 | 2 958 | 55 | –5.6 |
| 143-1-line7-1-4 | 0.210 | 0.003 | 16.42 | 0.22 | 0.567 | 0.007 | 0.67 | 61 | 279 | 0.218 | 2 905 | 39 | –0.2 |
| 143-1-line7-7-1 | 0.190 | 0.003 | 13.95 | 0.20 | 0.531 | 0.006 | 0.64 | 17 | 377 | 0.045 | 2 746 | 46 | 0.1 |
| 143-1-line7-9-2 | 0.203 | 0.003 | 14.84 | 0.21 | 0.531 | 0.006 | 0.65 | 92 | 174 | 0.526 | 2 848 | 45 | –3.6 |
| 143-1-line7-9-4b | 0.178 | 0.003 | 11.75 | 0.17 | 0.478 | 0.005 | 0.64 | 171 | 97 | 1.762 | 2 636 | 48 | –4.4 |

Notes: Rho is the error correlation coefficient. $^{207}Pb/^{235}U$ – $^{206}Pb/^{238}U$. D – degree of discordance: (((age by $^{206}Pb/^{238}U$)/(age by $^{207}Pb/^{206}Pb$)) – 1)*100.

## DISCUSSION

The combination of the obtained isotopic-geochemical characteristics of zircon grains, cathodoluminescence images of these crystals, and petrographic features of the rocks made it possible to identify patterns in the genesis of the studied zircon.

Cathodoluminescence images (CL) are a source of extensive information about the ontogenesis of zircon crystals and several other minerals that often do not have pronounced zonation in the optical range. The zonation of zircon crystals in cathodoluminescence and its relationship with crystallization conditions and processes have been intensively studied in recent decades. The obtained results allow making more or less confident conclusions about the genesis of this mineral (Nosyrev et al., 1989; Corfu et al., 2003; Kaulina, 2010). In particular, oscillatory zonation in zircon is considered as a sign of zircon crystallization from a melt in magmatic processes or during partial melting of rocks under conditions of high temperatures and pressures – for example, ultrametamorphism and the formation of migmatites or palingenesis (for example, Nosyrev et al., 1989). Sectorial zonation with serrated sector boundaries – of the "fir-tree" type – indicates zircon crystallization during metamorphism at relatively high temperatures – for example, under granulite facies conditions (Corfu et al., 2003; Kaulina, 2010).

To date, a large amount of data on the geochemistry of U and Th in zircon has been accumulated. It has been established that accessory zircon from rocks formed at temperatures and pressures of granulite facies is characterized by low concentrations of U and Th. (Bibikova, 1989; Nozhkin, Turkina, 1993). At the same time, the ratio of Th to U in zircon can vary from medium to high >1 (Rubatto et al., 2001; Kaulina, 2010; Harley et al., 2007). Under granulite facies conditions, thorium and uranium either exhibit similar geochemical behavior or separate due to the appearance of thorium-concentrating minerals, which is reflected in the Th/U value (Bea, 1996; Rubatto, 2017; Yakymchuk et al., 2018; Ewing et al., 2023).

Zircon from metamorphic rocks and migmatites of amphibolite facies, which is characterized by the presence of water-containing fluid, is distinguished by low – often below 0.1 – Th/U values (Glebovitsky et al., 2008), due to uranium's tendency to form complex

compounds (Nozhkin, Turkina, 1993). Thorium does not have the ability to be transported in aqueous fluid, so the presence of water-containing fluid during metamorphism can provide noticeable differences in the geochemical behavior of the elements under consideration (Hazen et al., 2009).

The patterns outlined above are used in the interpretation of the obtained results.

Thus, zircon from the sample of quartz diorites TB 238-4, belonging to the age interval of 3.04–2.98 (Fig. 5, Table 2), is divided into groups. Petrographic features of the rocks, morphology and structure of the internal zones of zircon crystals reflect crystallization from magma in *P–T* conditions and fluid regime corresponding to granulite and the boundary of amphibolite and granulite facies (for example, Fig. 4i (c – core), Table 2, Fig. 8, 238-4-4 and 238-4-9a). Uranium concentrations obtained for such crystals have relatively higher values and medium to elevated Th/U ratio (up to 1) (see the Results section and Table 2). Another group of analyzed grains, which include newly formed cores (for example, Fig. 4n, o, Fig. 8, 238-4-24 and 238-4-31) and the outer part of the grains of the first group (for example, Fig. 4i (r – rim), e, Table 2, Fig. 8, 238-4-9b) have lower uranium concentrations relative to the first group and average Th/U ratio (see the Results section and Table 2). Probably, in this time interval, several consecutive processes occurred, recorded in the structural features and geochemistry of zircon crystals. The first is the formation of primary igneous rocks, during which the conditions of zircon crystallization changed significantly, which is reflected in the differences in the structure of the outer and inner zones of the crystal cores. The second is the metamorphism of rocks under granulite facies conditions, expressed in the formation of crystals with sectorial zonation and "fir-tree" type

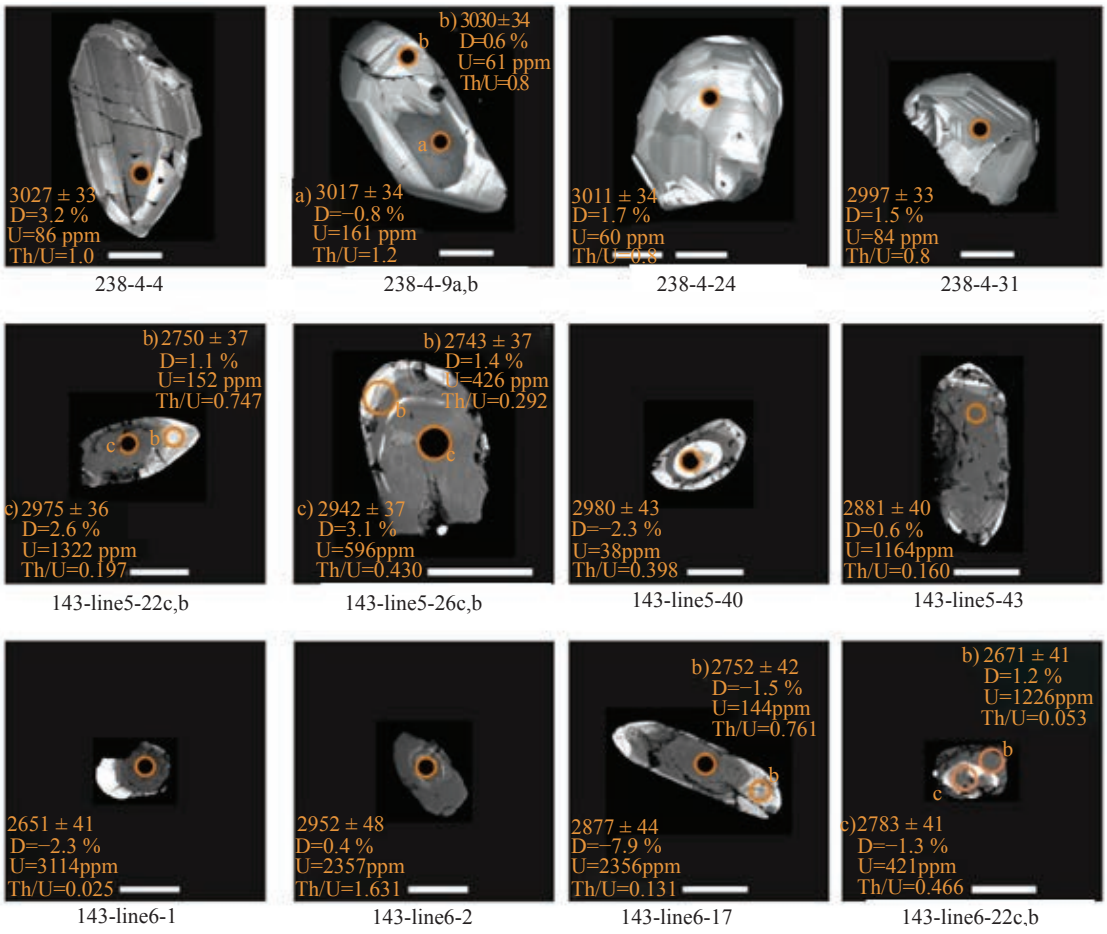


**Fig. 8.** Examples (cathodoluminescence images) of investigated zircon of different generations from weakly gneissic enderbites of the Otradnensky series (sample Pr 143-1) and metamorphosed quartz diorites of the Tanai plagiogranitoid massif (sample TB 238-4).
The grain numbers in the figure correspond to the point numbers presented in Tables 2 and 3, Appendices 1 and 2.

boundaries, shells on crystals of early generation (grains of the first type) with similar structural features. The above-mentioned igneous and metamorphic events, reflected in the formation of various generations of zircon from quartz diorites of the Tanai massif (sample TB 238-4), preserve the history of the primary rocks that were the substrate for the melting of quartz diorites.

The third, final process is the metamorphism of rocks under high-grade amphibolite facies conditions, reaching palingenic melting and formation of granitoid series rocks. Thus, in the quartz diorites under consideration, only mineral parageneses corresponding to *P–T* conditions of amphibolite facies metamorphism are observed. In zircon, this process is reflected in the formation of thin, dark gray in CL, "amphibolite" overgrowths on grains of the second, third and fourth types (see description of zircons). Since these processes are close in time, the error ellipses of the determined ages overlap (Fig. 5a), and the applied U–Pb dating methods do not allow to distinguish these processes.

Zircon from the quartz diorite sample TB 238-4 is characterized by low concentrations of U and Th, varying in a narrow range (Table 2) during transformation and change in the process regime under amphibolite and granulite facies conditions, both for the first group zircon of magmatic genesis and metamorphic zircon. It is likely that this is due to low concentrations of uranium and thorium during the formation of the plagiogranitoid Tanai massif, inherited from the protolith.

Analysis of the obtained isotope-geochronological data (zircon from the sample of weakly gneissic enderbites Pr 143-1) showed that in each of the identified narrow age intervals 3.0–2.8 billion years and 2.75–2.60 billion years, zircon grains of different generations are present. This indicates a multi-stage formation and transformation of rocks. Due to the multiplicity of such processes and their succession in a close time interval, we cannot unambiguously establish the sequence of these processes based solely on the morphology and internal structure of the grains. Granulite metamorphism and the immediately following regressive process are repeated at least twice. At the same time, zircon grains of different origins – magmatic and metamorphic genesis – fall into the same age interval. Their geochronological U–Pb isotopic determinations overlap within the range of errors. Therefore, zircon generations can only be distinguished by a combination of isotope-geochemical characteristics (U and Th content and Th/U ratio), structural features of grains manifested in CL images, and petrographic features of the rocks.

For the sample of weakly gneissic enderbites Pr 143-1 in the age range of 3.0–2.8 billion years, as well as for quartz diorites of the Tanai massif (Sample TB 238-4), there are several generations of zircon grains, whose ages overlap within the error margin, but are clearly differentiated by morphology and internal structure. The first generation consists of individual grains with cores that have a bright light color in CL images (for example, Fig. 6, grains 1a, 1b, 1c, 1d). They have low uranium and thorium content, average Th/U ratio, and show relict oscillatory zoning (Fig. 6 – 1a, 1b, Table 3, Fig. 8, 143-line5-40). The age of such zircon cores apparently corresponds to the crystallization of the protolith from magma. Probably, the preserved first generations of rock-forming minerals (antiperthitic *Pl* + *OPx*, Fig. 3b) were formed at this stage.

The next two generations of zircon (second and third) from the age range of 3.0–2.8 billion years have almost identical internal structure and grain morphology, differing only in Th, U contents and Th/U ratio.

The second generation of zircon grains has high U and Th content, and Th/U greater than 1 (for example, Fig. 6 – 2a, Table 3, Fig. 8, 143–line6-2). Such grains are characterized by a saturated gray tone of cathodoluminescence and a translucent uneven oscillatory zoning observed in the central parts of the grains. Their quantity in the studied sample is small, which may indicate a relatively low intensity and localized nature of this process. The high Th/U ratio and the presence of oscillatory zoning, which is a sign of crystallization from melt, allows us to assume their origin in the process of partial melting under *P–T* conditions of granulite facies. High U contents in zircon may be a consequence of a change in the fluid regime from "dry" to substantially water-bearing. This can be considered as an indication of changing conditions of crystallization or recrystallization of the rock and the zircon within it.

Zircon of the next, third generation, can be correlated with the process of transformation of primary enderbites into metamorphic rocks under conditions transitional between granulite and amphibolite facies. This zircon is characterized by high uranium concentrations and some decrease in Th/U ratio values relative to previous generations (down to 0.1–0.2) (for example, Table 3, Fig. 8, 143-line5-22c, 143-line5-43, 143-line6-17). Such characteristics indicate the presence of a water-containing fluid and a probable decrease in the temperature of the metamorphic process. Zircon of this generation has saturated homogeneous gray and dark gray tones in cathodoluminescence images with a complete

absence of zonation in the cores of such grains (Fig. 6, 2b–2d).

The age values of zircon from the interval of 2.75–2.60 billion years reflect the most prominently manifested process of granulite metamorphism, which gained regional distribution throughout the Volga-Ural segment. Within this age interval, a generation of zircon grains related to the granulite phase of metamorphism is distinguished (Fig. 6, 3a and 3c and rims in grains). The error ellipses for age determination of such crystals overlap with those values for the immediately succeeding process of regressive metamorphism. Their composition is characterized by relatively low U contents (on the order of one hundred ppm). The Th/U ratio in such crystals is above average (~0.7) and reaches values >1 (Table 3, Fig. 8, 143-line5-22b, 143-line5-26b, 143-line6-17b). Petrographically, this is reflected in the formation of gneissic structure of enderbites (Fig. 3a, c).

The regressive stage of the above-described regional metamorphism of amphibolite facies is marked by the formation of thin dark gray in CL zircon rims and crystals with homogeneous gray cores (Fig. 6, 4a–d). Zircon of such generation is characterized by high U contents (thousands of ppm) and extremely low Th/U ratios <0.1 to 0.01 (Table 3, Fig. 8, 143-line6-1, 143-line6-22b).

One can speak of the location of groups of zircon age values from the sample of weakly gneissic enderbites Pr 143–1 in two main ranges (Fig. 7, 9, 10), described above.

The processes of crystallization and recrystallization of zircon from the sample of slightly gneissic enderbites Pr 143-1 and, accordingly, the stages of formation and transformation of the rock occurred repeatedly and were close in time. First, each group of values of the obtained isotopic ratios corresponds to a group of analysis points of zircon zones and crystals that differ sharply in radiation characteristics in cathodoluminescence mode (Fig. 6). Second, the values of U and Th concentrations, Th/U ratios in different zircon grains and zones differ sharply (Table 3, Fig. 8, Fig. 9, inset, Fig. 10). At the same time, the age values obtained from isotopic ratios measured in different crystal zones may overlap within error limits (Fig. 8, 9). Thus, zircon from each time range marks processes related specifically to this established time interval.

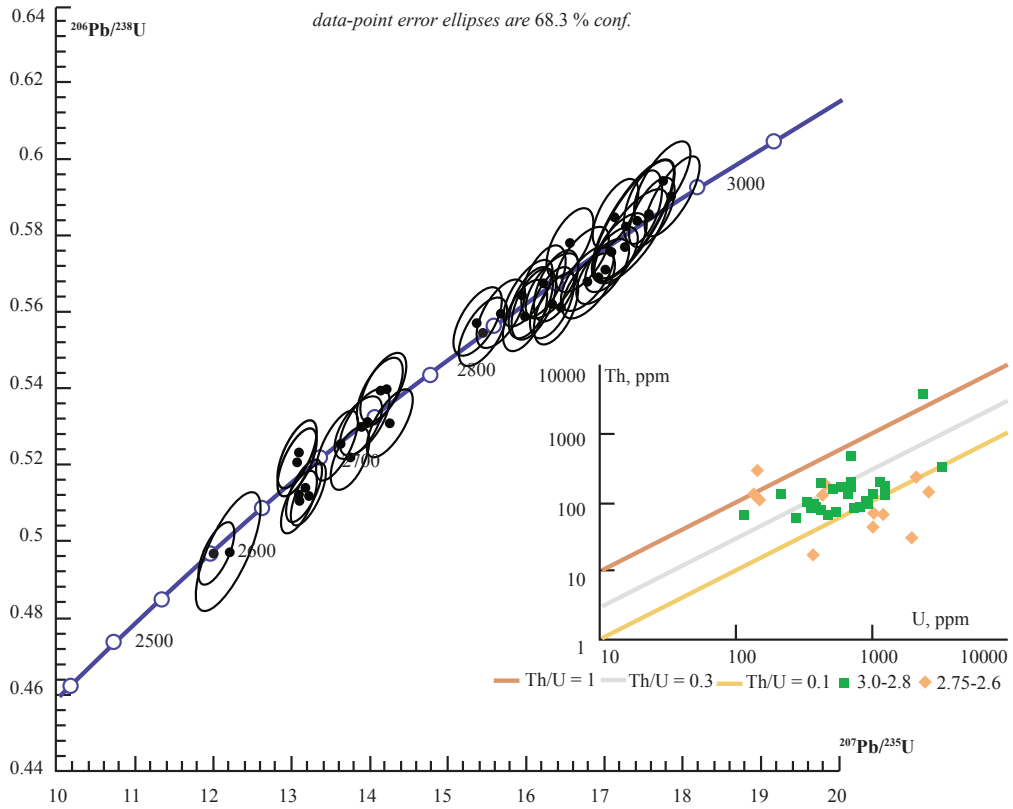


**Fig. 9.** Concordia diagram for zircon points (D < 2%) from the sample of slightly gneissic enderbites Pr 143-1 and distribution of points (D < 2%) from age intervals 3.0–2.8 and 2.75–2.60 billion years (values calculated from isotopic ratio $^{207}Pb/^{206}Pb$) in U–Th coordinates.

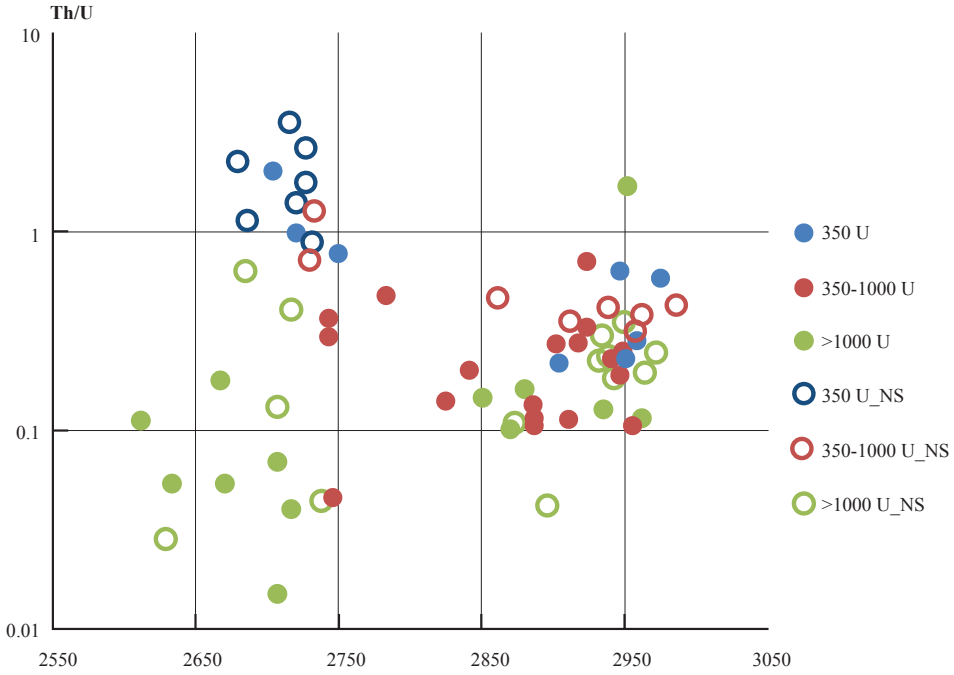


**Fig. 10.** Distribution of zircon points (by U content, ppm) from the sample of slightly gneissic enderbites Pr 143-1 of different generations by age determined from isotopic ratio $^{207}Pb/^{206}Pb$ (D < 2%) depending on Th/U. Filled symbols – determinations by LA-ICP-MS method, unfilled symbols – determinations on Cameca IMS 1280 Nordsim secondary ion mass spectrometer (SIMS) according to the methodology of Whitehouse & Kamber (2005), shown for comparison.

## CONCLUSION

The most significant stages of crustal formation and the age of the main rock complexes of the Middle Volga block have been substantiated by a number of previous studies. The Archean time of origin and metamorphic transformation of the sialic crust of the Kama-Vyatka zone of the Volga-Ural segment has been determined and substantiated for the first time. Using the example of accessory zircon from repeatedly metamorphosed primary igneous rocks of the Kama-Vyatka zone of the Volga-Ural segment of the East European Craton, the patterns of formation of zircon zones have been studied, each of which corresponds to a certain stage of crystallization and/or recrystallization of enderbites of the Otradnensky series and plagiogranitoid rocks of the Tanai massif as a result of polymetamorphic processes.

Zircon isolated from quartz diorites showed the Archean time of formation of the protolith of plagiogranitoids of the Tanai massif of the Kama-Vyatka zone. This age interval – 3.04–2.98 billion years – includes the stage of the earliest granulite metamorphism, immediately following the episode of magmatism.

Two age intervals of rock formation and transformation were obtained from zircon from weakly gneissic enderbites of the Otradnensky series: 3.0–2.8 billion years and 2.75–2.60 billion years.

In the age interval of 3.0–2.8 billion years, zircon marks the following events: crystallization from magma of primary enderbites, ultrametamorphism (including partial melting of low degrees) of granulite facies, and a regressive stage that occurred in the boundary conditions of granulite and amphibolite facies. The age of the oldest magmatic zircon population is 3.0–2.8 billion years, which determines the age of melting of the primary enderbites of the Otradnensky series. Taking into account the model age of enderbites, the age of the Otradnensky series of the Kama-Vyatka zone of the Volga-Ural segment was estimated for the first time at 3.0 ± 0.1 billion years.

In the age range of 2.75–2.60 billion years, zircon records the most powerful episode of granulite metamorphism, widely manifested throughout the Volga-Ural segment, followed by regressive metamorphism of the amphibolite facies. The combination of data from the region (Bibikova et al., 1984, 1994, 2015; Bogdanova et al., 2010) and the obtained results from zircon in the sample of weakly gneissified enderbites Pr 143-1 of the Otradnaya series allows us to assert that the interval of 2.75–2.60 billion years corresponds to the maximum manifested episode of granulite

metamorphism and corresponds to the time of stabilization of the continental crust of the Kama-Vyatka zone and the Middle Volga block of the Volga-Ural segment.

During a long formation history, mineral parageneses typically reflect the most recent rock alterations. Zircon, being a stable mineral, often records the most ancient high-temperature transformations and can be inert to superimposed processes, reflecting history fragmentarily. Reconstructing a continuous sequence of rock alteration stages is only possible through comprehensive research of rock mineral parageneses and zircon. This study showed that reconstructing the history of rock formation and transformation should be conducted by studying zircon in conjunction with the petrographic features of its host rocks.

## ACKNOWLEDGEMENTS

The authors express gratitude for assistance in conducting research and working with the TESCAN MIRA 3 electron microscope to S.I. Demidova, as well as for consultations and discussion of results to Yu.A. Kostitsyn, V.B. Polyakov and A.V. Somsikova, M.V. Luchitskaya, and to the scientific editor A.B. Kuznetsov.

## FUNDING

The research was carried out under the State Assignment of the Vernadsky Institute of Geochemistry and Analytical Chemistry of the Russian Academy of Sciences.

## REFERENCES

1. *Bibikova E.V.* (1989) Uranium-lead geochronology of early stages of ancient shields development. Moscow. Nauka.
2. *Bibikova E.V., Bogdanova S.V., Larionov A.N., Fedotova A.A., Postnikov A.V., Popova L.P., Kirnozova T.I., Fugzan M.M.* (2008) New data on the Early Archean age of granitoids of the Volga-Ural segment of the East European craton. *DAN*. 419 (2), 219–223.
3. *Bibikova E.V., Bogdanova S.V., Postnikov A.V., Fedotova A.A., Claesson S., Kirnozova T.I., Fugzan M.M., Popova L.P.* (2015) Early crust of the Volga-Ural segment of the East European craton: isotope-geochronological study of terrigenous zircon from metasedimentary rocks of the Bolshaya Cheremshana series and their Sm–Nd model age. *Stratigraphy. Geological Correlation*. 23 (1), 1–24.
4. *Bibikova E.V., Bogdanova S.V., Kirnozova T.I., Popova L.P.* (1984) Uranium-lead age of charnockitoids in the Volga-Ural region. *Doklady Akademii Nauk SSSR*. 276 (4), 916–919.
5. *Bibikova E.V., Kirnozova T.I., Popova L.P., Postnikov A.V., Makarov V.A., Kremenetsky A.A.* (1994) U–Pb age and correlation of magmatic formations of granulite and amphibolite complexes of the Volga-Ural region of the East European Craton. *Stratigraphy. Geological Correlation*. 2 (3), 3–7.
6. *Bogdanova S.V.* (1986) The Earth's crust of the Russian plate in the Early Precambrian (using the example of the Volga-Ural segment). *Proceedings of GIN AN SSSR*. 408p.
7. *Glebovitsky V.A., Sedova I.S., Matukov D.I., Berezhnaya N.G., Tolmacheva E.V., Samorukova L.M.* (2008) Geochemistry and geochronology of migmatites of the Kurultino-Nyukzha segment and problems of correlation of metamorphic events in the Dzhugdzhur-Stanovoy folded region, Eastern Siberia. *Petrology*. 16 (6), 627–656.
8. Pre-platform complexes of oil and gas bearing territories of the USSR. (1992) eds. Knyazev V.S. and Lapinskaya T.A. Moscow: Nedra. 309 p.
9. *Kaulina T.V.* (2010) Formation and transformation of zircon in polymetamorphic complexes. Apatity: Publishing House of the Kola Science Center RAS.
10. *Kostitsyn Yu.A., Anosova M.O.* (2013) U–Pb age of extrusive rocks of the Uksichan caldera in the Sredinny Range of Kamchatka – application of laser ablation for dating young zircons. *Geochemistr*. (2), 171–179.
11. *Kostitsyn Y.A., Anosova M.O.* (2013) U–Pb age of extrusive rocks in the Uxichan caldera, Sredinnyi Range, Kamchatka: Application of laser ablation in dating young zircons. *Geochem. Int.* 51 (2), 155–163.
12. *Lapinskaya T.A., Bogdanova S.V.* (1976) Main features of the geological structure and major metamorphic and igneous complexes of the Precambrian basement of the Volga-Ural oil and gas-bearing region. *Geology, petrology and metallogeny of crystalline formations of the East European Craton*. Moscow. Nedra. 1, 106–115.
13. *Nozhkin A.D., Turkina O.M.* (1993) Geochemistry of granulites of Kansk and Sharyzhalgai complexes. *Proceedings of OIGGM*. 817. Novosibirsk: OIGGM SB RAS.
14. *Nosyrev I.V., Robul V.M., Esipchuk K.E., Orsa V.I.* (1989) Generational analysis of accessory zircon. Moscow: Nauka.
15. *Revyako N.M., Kostitsyn Yu.A., Bychkova Ya.V.* (2012) Interaction of mafic melt with host rocks during the formation of the Kivakka layered intrusion, North Karelia. *Petrology*. 20 (2), 115–135.
16. *Taylor S.R., McLennan S.M.* (1988) Continental crust, its composition and evolution: Translation from English, Moscow: Mir.

**17.** *Fedotova A.A., Bogdanova S.V., Claesson S., Anosova M.O., Postnikov A.V., Fugzan M.M., Kirnozova T.I.* (2019) New data on the Paleoproterozoic age of metamorphism in the Elabuga deformation zone of Volgo-Uralia, East European Craton. *DAN*. 488 (3), 307–312.

**18.** *Bea F.* (1996). Residence of REE, Y, Th and U in Granites and Crustal Protoliths; Implications for the Chemistry of Crustal Melts. Journal of Petrology. 37 (3), 521–552.

**19.** *Belousova E.A., Kostitsyn Y.A., Griffin W.L., Begg G.C., O'Reilly S.Y., Pearson N.J.* (2010) The growth of the continental crust: Constraints from zircon Hf-isotope data. *Lithos* . 119, 457–466.

**20.** *Bogdanova S.V.,* (1993) The three-segment hypothesis of the East European Craton. *Terra Nova*. 5, 313–314.

**21.** *Bogdanova S.V., Gorbatschev R., Garetsky R.G.* (2016) EUROPE|East European Craton. Reference Module in Earth Systems and Environmental Sciences. Elsevier, 34–49.

**22.** *Bogdanova S.V., De Waele B., Bibikova E.V., Belousova E.A., Postnikov A.V., Fedotova A.A., Popova L.P.* (2010) Volgo-Uralia: the first U–Pb, Lu–Hf, and Sm–Nd isotopic evidence of preserved Paleoarchean crust. *Am. J. Sci*. 310, 1345–1383.

**23.** *Chauvel C., Garçon M., Bureau S., Besnault A., Jahn Bor-ming, Ding Zh.* (2014). Constraints from loess on the Hf–Nd isotopic composition of the upper continental crust. *Earth Planet. Sci. Lett.* 388, 48–58.

**24.** *Condie K.C.* (2018) A planet in transition: The onset of plate tectonics on Earth between 3 and 2 Ga? *Geoscience Frontiers*. 9, 51–60.

**25.** *Corfu F., Hanchar J.M., Hoskin P.W.O., Kinny P.* (2003) Atlas of zircon textures. *Rev. Mineral. Geochem.* 53, 469–500.

**26.** *Ewing R.C., Meldrum A., Wang L, Weber W.J., Corrales L.R.* (2003) Radiation Effects in Zircon. *Rev. Mineral. Geochem.* 53, 387–425.

**27.** *Ewing T., Rubatto D., Lemke K., Hermann J.* (2023) Timescales and mechanisms of felsic lower continental crust formation: Insights from U Pb geochronology of detrital zircon (Malenco Unit, eastern Central Alps). *Lithos*. 456–457, 107286.

**28.** *Harley S.L., Kelly N.M., Möller A.* (2007) Zircon behavior and the thermal histories of mountain chains. *Elements*. 3, 25–30.

**29.** *Hawkesworth Chris J., Cawood P.A. and Dhuime B.* (2020) The Evolution of the Continental Crust and the Onset of Plate Tectonics. *Frontiers in Earth Science*. 8, 326, 1– 23.

**30.** *Hawkesworth C.J., Dhuime B., Pietranik A., Kemp A.I.S., Storey C.D.* (2010) The generation and evolution of the continental crust. *J. Geol. Society*. 167, 229–248.

**31.** *Hazen R., Ewing R., Sverjensky D.* (2009) Evolution of uranium and thorium minerals. *American Mineralogist*. 94, 1293–1311.

**32.** *Jackson S.E., Pearson N.J., Griffin W.L., Belousova E.A.* (2004) The application of laser ablation–inductively coupled plasma-mass spectrometry to in situ U–Pb zircon geochronology. *Chem. Geology*. 211, 47–69.

**33.** *Kohn M. & Kelly N.* (2018) Petrology and Geochronology of Metamorphic Zircon (in: Microstructural Geochronology: Planetary Records Down to Atom Scale. Eds.: Moser D., Corfu F., Darling J., Reddy S., Tait K.), 35–61. doi.org/10.1002/9781119227250.ch2

**34.** *Kunz B., Regis D., Engi M.* (2018) Zircon ages in granulite facies rocks: decoupling from geochemistry above 850°C? *Contrib. Mineral. Petrol.* 173, 26.

**35.** *Ludwig K.R.* (2008) Isoplot V. 4.15. Geochronological Toolkit for Microsoft Excel. *Berkeley Geochronol. Center, Spec. Publ*. (4).

**36.** *Rubatto Daniela.* (2017) Zircon: The Metamorphic Mineral. *Rev. Mineral. Geochem.* 83 (1), 261–296.

**37.** *Rubatto D., Gebauer D.* (2000) Use of Cathodoluminescence for U–Pb Zircon Dating by Ion Microprobe: Some Examples from the Western Alps. M. Pagel et al. (eds.), Cathodoluminescence in Geosciences. Berlin – Heidelberg: Springer-Verlag, 373–400.

**38.** *Rubatto D., Williams I. and Buick I.* (2001) Zircon and monazite response to prograde metamorphism in the Reynolds Range, Central Australia. *Contrib. Mineral. Petrol*. 140, 458–468.

**39.** *Tanaka T., Togashi S., Kamioka H. et al.* (2000) JNdi-1: a neodymium isotopic reference in consistency with LaJolla neodymium. *Chem. Geol*. 168 (3–4), 279–281.

**40.** *Taylor S.R. & McLennan S.M.* (2009) Planetary crusts: Their composition, origin and evolution. Cambridge: Cambridge University Press.

**41.** *van Achterbergh E., Ryanm C.G., Griffin W.L.* (1999) GLITTER: On-line interactive data reduction for the laser ablation ICP-MS microprobe. Proc. the 9th Goldschmidt Conf. Cambridge, Massachusetts, 305.

**42.** *Whitehouse M.J. & Kamber B.S.* (2005) Assigning dates to thin gneissic veins in high#grade metamorphic terranes: a cautionary tale from Akilia, Southwest Greenland. *J. Petrol*. 460, 291–318.

**43.** *Wiedenbeck M., Allé P., Corfu F., Griffin W.L., Meier M., Oberli F., Quadt A.V., Roddick J.C., Spiegel W.* (1995) Three Natural Zircon Standards for U–Th–Pb, Lu–Hf, Trace Element and REE Analyses. *Geostand. Newsletters*. 19, 1–23.

**44.** *Yakymchuk C., Kirkland C., Clark C.* (2018) Th/U ratios in metamorphic zircon. *J. Metamorph. Geol*. 36 (6), 715–737.